64-5

ARL 63-165

TRANSIENT DISCHARGES IN WHIRL STABILIZED ARCS

K. H. HOCKER
K. MAILANDER
E. PFENDER
H. SCHRADE
H. P. STREIBLE
W. THIELO

INSTUTUT FUR HOCHTEMPERATURFORSCHUNG
DER TECHNISCHEN HOCHSCHULE STUTTGART

JUNE 1963

AERONAUTICAL RESEARCH LABORATORIES
OFFICE OF AEROSPACE RESEARCH
UNITED STATES AIR FORCE

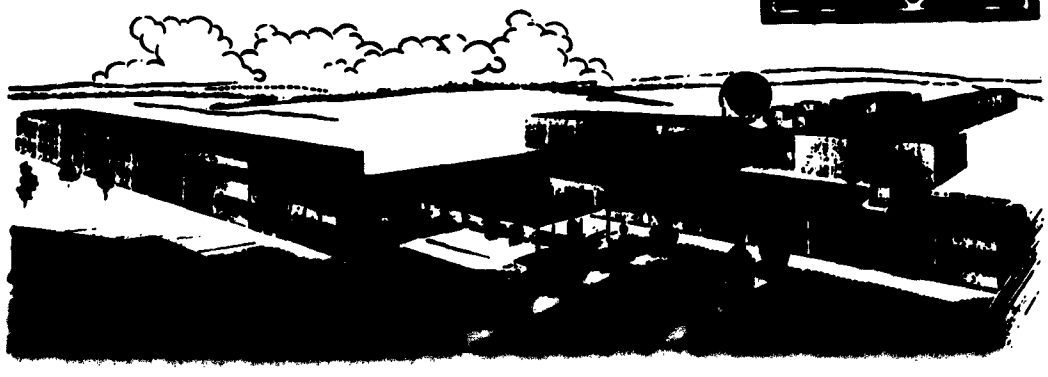

NOTICES

When Government drawings, specifications, or other data are used for any purpose other than in connection with a definitely related Government procurement operation, the United States Government thereby incurs no responsibility nor any obligation whatsoever; and the fact that the Government may have formulated, furnished, or in any way supplied the said drawings, specifications, or other data, is not to be regarded by implication or otherwise as in any manner licensing the holder or any other person or corporation, or conveying any rights or permission to manufacture, use, or sell any patented invention that may in any way be related thereto.

- - - - - - - - - -

Qualified requesters may obtain copies of this report from the Armed Services Technical Information Agency, (ASTIA), Arlington Hall Station, Arlington 12, Virginia.

- - - - - - - - - -

This report has been released to the Office of Technical Services, U. S. Department of Commerce, Washington 25, D. C. for sale to the general public.

- - - - - - - - - -

Copies of ARL Technical Documentary Reports should not be returned to Aeronautical Research Laboratory unless return is required by security considerations, contractual obligations, or notices on a specific document.

200 - October 1962 - 8-141-162

Aeronautical Research Laboratories, Wright-Patterson AFB,O. TRANSIENT DISCHARGES IN WHIRL STABILIZED ARCS by K.H. Hocker, et al, Technishen Hochschule, Stuttgart, Germany. June 1963. 79 p. incl.illus. (Project 7073;Task7073-01) (Contract AF 61 (052)-590) (ARL 63-105)
Unclassified Report

Experiments were conducted to study the problem of heating and stability of pulsed discharges. In order to have reproducible conditions and defined geometry a pre-discharge representing a highly ionized plasma

(over)

UNCLASSIFIED

was used and described. Then, the basic equations for the heating process which were developed in our institute and the main features of a model which allows to apply them to a cylindrical discharge are summarized.

UNCLASSIFIED

Aeronautical Research Laboratories, Wright-Patterson AFB,O. TRANSIENT DISCHARGES IN WHIRL STABILIZED ARCS by K.H. Hocker, et al, Technishen Hochschule, Stuttgart, Germany. June 1963. 79 p. incl.illus. (Project 7073;Task7073-01) (Contract AF 61 (052)-590) (ARL 63-105)
Unclassified Report

Experiments were conducted to study the problem of heating and stability of pulsed discharges. In order to have reproducible conditions and defined geometry a pre-discharge representing a highly ionized plasma

(over)

UNCLASSIFIED

was used and described. Then, the basic equations for the heating process which were developed in our institute and the main features of a model which allows to apply them to a cylindrical discharge are summarized.

UNCLASSIFIED

ARL 63-105

TRANSIENT DISCHARGES IN WHIRL STABILIZED ARCS

K. H. HOCKER
M. MAILANDER
E. PFENDER
H. SCHRADE
H. P. STREIBLE
W. THIELO

INSTUTUT FUR HOCHTEMPERATURFORSCHUNG
DER TECHNISCHEN HOCHSCHULE STUTTGART

JUNE 1963

Contract AF 61(052)-590
Project 7073
Task 7073-01

The research reported in this document has been sponsored in part by the Aeronautical Research Laboratory, OAR through the European Office, Aerospace Research, United States Air Force.

Foreword

This final report was prepared by the Institut für Hochtemperaturforschung, Technische Hochschule Stuttgart, Germany on Contract AF 61 (052)-590 for the Aeronautical Research Laboratories, Office of Aerospace Research, United States Air Force. The work reported herein was accomplished under the technical cognizance of Dr. Rolf Ammann, Branch Chief and Dr. W.G. Braun, Project Scientist of the Plasma Physics Branch of ARL.

The investigations consist of

1) production of plasmas
2) diagnostics of discharges
3) calculations of the heating process and stability problems

The authors gratefully acknowledge the help of Dr. W. Bez, who directed the fundamentals of the scientific work reported here before leaving for 15 months to ARL. Dipl.Ing. K. Schreitmüller and Dipl.Ing. H.H. Maier have performed the technical equipment and short time diagnostics. M. Kling has spent much effort in constructing a vacuum sluice for the vacuum spectrograph.

Abstract

Experiments were conducted to study the problem of heating and stability of pulsed discharges. In order to have reproducible conditions and defined geometry a pre-discharge representing a highly ionized plasma was used and described. Then, the basic equations for the heating process which were developed in our institute and the main features of a model which allows to apply them to a cylindrical discharge are summarized.

The impulse discharge is described in nitrogen as well as in hydrogen. As there is a quasi-stability in nitrogen but not in hydrogen - in accordance with theory - the experimental investigation of the nitrogen discharge gives definite results. The maximum temperature reached is about 80 000 ^{o}K.

The main task is the development of diagnostic tools for investigation of short time phenomena in dense plasmas.

In this field, suitable magnetic probes of very small dimensions were developed. In addition, an apparatus was constructed which allowed to shoot the probes into the discharge channel. The possible disturbance of the plasma channel was carefully studied. We succeeded in getting temperature and current profiles of this discharge as well as precise figures of the development with time.

Another diagnostic method is short time spectroscopy. We used the visible region as well as the UV and the vacuum UV. The results of the visible and UV-spectroscopy agree with the probe data. Our efforts for gaining even more information by vacuum spectroscopy are still engaged with the development of the experimental procedure, which is described in principle.

Concerning hydrogen heating, the discharge is highly instable. The reasons for this relatively to nitrogen are revealed by theory. We discuss in which way the discharge conditions should be altered to get a quasi stable heating process which will give about several hundred thousand degrees.

Contents

I. Introduction and Survey

The highest temperatures which could be achieved stationary so far by means of suitable arcs amount to 50 000 ^{o}K. In theory, the plasmas of these arcs represent a quasi-thermodynamic equilibrium of the matter. It is possible that, for short times, somewhat higher electron temperatures were obtained in spark discharges. But in this case there exists no longer a thermodynamic equilibrium. The ion temperatures are considerably lower. The recent plasma research aims at extremely high temperatures, such as 10^{8} ^{o}K for the ion component. But there are many experimental difficulties which are opposed to this. Nevertheless, the temperatures which could be achieved so far provide a chance to realize the direct conversion of thermal energy into electric energy with good efficiency. In these efforts, the properties of flowing plasmas in electric and magnetic fields must be well known. One of the most fundamental problems in all future developments is the Ohmic heating process. Studying it without considering any application means to provide physicists and engineers with the highly elementary and most important knowledge on the characteristic interaction between electrons and ions in the electric and magnetic field, the energy balance, the stability as well as the magnetic confinement of the plasmas.

The following work provides a comprehensive description of our investigations on the Ohmic heating. Experimentally, they are based on a high current impulse discharge over a gas vortex stabilized high temperature arc in nitrogen and hydrogen atmosphere. The theory deals with a channel model which corresponds to the experiment. The transmission of the energy obtained in the electric field to thermal motion due to scattering is studied, possible energy losses are considered. This mechanism determines the radius of the current carrying plasma channel and thus the magnetic compression. The ratio of this compression to the gas-kinetic pressure decides on the stability of the discharge.

The stable and quasi-stable discharges are measured by means of magnetic probes. Their production and arrangement in the hot discharge channel by means of a "probe gun" is described. With the aid of the probes the radial current and temperature profiles of impulse discharges in nitrogen are determined. Moreover, the heating of the plasma channel can be observed with time. The probe measurements well agree with spectroscopic measurements in the visible and UV-ranges. In addition they allow a profound discussion of the heating mechanism and radiation transport from the center of the discharge to the boundary region, being connected with the creation of charge carriers and enlarging the discharge channel.

Furthermore we tried to develop another method providing information about the behaviour of high temperature plasmas. For this purpose, a vacuum spectrograph was used. So far it has not yet been possible to carry out reproducible measurements of stationary arcs and impulse discharges by means of the vacuum spectrograph. As this technique is still rather undeveloped, we first had to carry out an analysis of the lines suitable for spectroscopic measurements and then to develop an apparatus with different steps for the transition from the dense medium of the discharge to the vacuum of the spectrograph. The progress of this is described.

Most of the transient discharges with high current densities are in principle unstable. The instabilities have a characteristic developing time in which they appear. This time mainly depends on the viscosity of the plasma and the transition to the cold rotating outer gas. It can be longer or shorter than the time of a halfwave of the condenser discharge. In the first case a quasi-stability is the result. This applies to our nitrogen discharges, while the impulses in hydrogen prove to be strongly unstable. The calculations show in which direction the discharge conditions should be altered in order to obtain here quasi-stable discharges.

The observation of the instabilities is based on image converter information as well as on fotating mirror technique and framing camera pictures. The instability is con-

firmed by all methods. However, in detail the statements are different. This suggests the assumption that the image converter photographs depend on the frequency in an unknown way. Systematic investigations along these lines would be highly desirable.

II. The Ohmic Heating Process

1. Pre-discharge in nitrogen and hydrogen

In theory and experiment we wish to have a starting point as clear as possible. In the heating process, this means that electrons and ions should be present when acceleration of particles begins. Therefore, we start from a highly pre-ionized discharge channel. In addition we fix the discharge gap for the following impulse discharge by means of the pre-ionized channel. The pre-ionized channel is represented by an arc which by means of a gas vortex is narrowed and stabilized, its temperature is rather high. The gas vortex prevents the lift of the discharge channel which is usually observed. The axis temperature of the discharge channel in nitrogen is about 12 000 ^{o}K, in hydrogen above 20 000 ^{o}K. Fig. 1 shows a cross section through our experimental arrangement. It had to fulfill very high thermal and mechanic conditions over several minutes. The cooling was the main problem. Fig. 2 shows a characteristic photograph of the vortex stabilized arc. In case of black-white photography it is the same for nitrogen and hydrogen. The electrode distance and chamber diameter are 3 cm each. The diameter of the discharge channel is between 2 and 3 mm, the pressure amounts to about 1 at. The experimental arrangement was used for both nitrogen and hydrogen discharges.

For nitrogen the arc channel is stable, which could be proved by Fastax camera photographs (8 000 images per second).

It is described in more detail by K.H. Höcker and W. Kluge (1959)..Our theoretical stability investigations, carried out by H.E. Wilhelm (1962) confirm this result. In the case of hydrogen the Fastax camera photographs show fluctuations around the zero adjustment, their frequency being about 1 K.c. (E. Pfender and W. Bez, 1961; E. Pfender, 1962).

The investigation of the radial temperature distribution of the discharge channel was first done by means of spectroscopic measurements. Fig. 3 and 4 show the radial temperature distribution for two gas flow rates. In the case of the nitrogen arc the radial temperature distribution was estimated by means of the band spectra, atom and ion spectral lines, varying with the radius. In addition, this was controlled with the aid of another method (Inglis-Teller) consisting of an admixture of hydrogen. H_α -, H_β- and H_γ-lines appear. This yields an electron density of $5 \cdot 10^{17}$ cm^{-3}, which at a pressure of 4 at corresponds to an ionization degree of 20 % and the already mentioned axis temperature of about 12 000 ^oK (Mailänder, 1961).

The temperature of the hydrogen arc was determined from the broadening of the H - lines and the absolute measurement of the Balmer continuum. In addition to the Inglis Teller approximation was applied: Hydrogen lines up to H_ε could be observed. This yields an axis temperature above 20 000 ^oK (R. Schneider, 1961 c). This value includes an integration over the fluctuations.

2. Basic Equations for the Heating Process.

In order to provide a consequent calculation of the particles energy in our discharge, H.J. Kaeppeler (1958) and Schrade, Bez, Kaeppeler, Höcker (1960) have extended the 13 moments approximation of the Boltzmann equation first derived by H. Grad (1949). They are valid for each individual component of the plasma and read in a form including magnetic interaction:

a) conservation law for the mass density ρ_s, continuity equation:

$$\frac{\partial}{\partial t}\rho_s + \frac{\partial}{\partial \vec{r}} \cdot \left(\rho_s \vec{v}_s\right) = \left\{\frac{\partial}{\partial t}\rho_s\right\}_{col} \quad (1)$$

b) Conservation law for the impulse density $\vec{i}_s$, equation of motion:

$$\frac{\partial}{\partial t}\vec{i}_s + \frac{\partial}{\partial \vec{r}}\left\{\left(\vec{v}_s \vec{i}_s\right) + P_s\right\} - \rho_s \frac{z_s e}{m_s}\left[\vec{E} + \frac{1}{c}\vec{v}_s \times \vec{B}\right] = \left\{\frac{\partial}{\partial t}\vec{i}_s\right\}_{col} \quad (2)$$

c) Conservation law for the thermal energy density $u_s = c_v T_s$, thermal energy equation:

$$\frac{\partial}{\partial t}u_s + \frac{\partial}{\partial \vec{r}}\left(\vec{v}_s u_s\right) + \frac{\partial}{\partial \vec{r}} \cdot \vec{q}_s + P_s : \frac{\partial}{\partial \vec{r}}\vec{v}_s = \left\{\frac{\partial}{\partial t}u_s\right\}_{col} \quad (3)$$

Here $\vec{v}_s$ is the mean mass velocity of the component s, P_s the pressure tensor and $\vec{q}_s$ the heat transfer vector of this component. $\left\{\frac{\partial}{\partial t}\phi\right\}_{col}$ is the expression for the change of ϕ which is caused by collisions.

P_s and $\vec{q}_s$ must be calculated as function of n_s, $\vec{v}_s$, T_s, the gradient of these and the field quantities. Hirschfelder and others (1953) have dealt with the problem for non-ionized gases. Several authors, among them ourselves, extended it to plasmas, including strong electric and magnetic fields (details cf. H. Schrade, 1963).

The expression in parenthesis { } on the right of the equations (1-3) are called collision integrals and represent the interaction of the individual components. The bracket expression in the continuity equation considers the change of the mass density of the component s, which is due to reaction collisions. Taking into account the photoionization, the photorecombination, the collision ionization and the triple collision recombination, the collision integral for the ionization degree i is:

$$\left\{\frac{\partial}{\partial t} n_i\right\} = n_{i-1} Q_{i-1,i} - n_i n_e Q_{i,i+1} + n_{i-1} n_e S_{i-1,i} - n_i n_e^2 \underset{(4)}{S_{i,i-1}}$$
$$- n_i Q^{ul}_{i,i+1} + n_{i+1} n_e Q_{i+1,i} - n_i n_e S_{i,i+1} + n_{i+1} n_e^2 S_{i+1,i}$$

n_e, n_i are the electron and ion densities ($= \rho_{e,i}/m_{e,i}$) with the following reaction coefficients:

$Q_{i-1,i}$	and	$Q_{i,i+1}$	for the photoionizations,
$Q_{i,i-1}$		$Q_{i+1,i}$	for the photorecombinations,
$S_{i-1,i}$		$S_{i,i+1}$	for the collision ionizations,
$\beta_{i,i-1}$		$\beta_{i+1,i}$	for the triple collision recombinations.

They are mainly functions of the electron temperature and ionization energy. The photoionization coefficient in addition depends on the radiation intensity and thus represents the interaction between radiation field and particle. The reaction coefficients are calculated from the formulas of Elwert (1952) and Knorr (1958).

If the temperature is changed quickly, the numbers of ionizations and recombinations will be different from each other. The particle composition does no longer result from the equilibrium conditions, as do the Saha-equation and Korona-condition, but must be calculated exactly from equation (4). If i = 0, that means if we consider neutral particles and their interactions with electrons and ions, we get

$$-\frac{\frac{dn_0}{dt}}{n_0} = n_e Q_{0,1} - \frac{n_1}{n_0} n_e Q_{1,0} + n_e S_{0,1} - \frac{n_1}{n_0} n_e^2 S_{1,0} = \quad (5)$$

$$\frac{1}{\tau_{0\,\mathrm{Reakt.}}}$$

The right hand side of this equation may be defined as the reciprocal relaxation $\tau_{0\ \mathrm{Reakt}}$. If the above equation is applied on our experiments ($n_e = 10^{16}$ cm^{-3}, $n_1/n_0 = 10^{-2}$, T = 10 000 °K, heating the electrons up to 40 000 °K), we obtain $\tau_{0\ \mathrm{Reakt}} \gg 10^{-7}$ s. This can not be neglected compared to the heating time.

The collision integral in the equation of motion has the dimension of a force per unit volume and can be regarded as a frictional force density. Assuming that in the electric

field ions and electrons penetrate each other, both gases are moderated by mutual collisions. This behaviour is described by a frictional force being defined by the mean loss of impetus per collision multiplied with the number of collisions per s and cm^3:

$$\vec{R}_{ei} = \iiint m_e(\vec{v}'_e - \vec{v}_e) f_e f_i g a b_{ei} \, db_{ei} \, d\varphi \, d\vec{v}_i \, d\vec{v}_e \tag{6}$$

The mean thermal electron velocity being much larger than the mean diffusion velocity, the collision integral is calculated as follows

$$\left\{\frac{\partial}{\partial t}\vec{i}_e\right\}_{coll} = \sum \vec{R}_{ei} = -\sum n_e n_\nu \varepsilon_{e\nu}(\vec{v}_e - \vec{v}_\nu) \tag{7}$$

with

$$\varepsilon_{e\nu} = \frac{8}{3\sqrt{\pi}} m_e \sqrt{\frac{2KT_e}{m_e}} Q_{e\nu} \tag{8}$$

$Q_{e\nu}$ is the elastic scattering cross section between electrons and particles of the kind ν; $\nu = i$ is the cross section for electron ion-collisions

$$Q_{ei} = \frac{Z_i^2 e^4}{k^2 T_e^2} \cdot \frac{\tilde{\pi}}{4} \ln \frac{9}{4\pi} \frac{(KT_e)^3}{Z^2(Z+1)e^6 n_e} \tag{9}$$

---

*) The above requirement corresponds to the usual requirements of thermal plasmas. If this condition is not fulfilled, we get two-stream instabilities. E.A. Jackson (1960) and D.A. Tidman (1961).

The collision integral in the energy equation of electrons is:

$$\left\{\frac{\partial}{\partial t}u_e\right\}_{coe} = \frac{j^2}{\sigma} - \sum_\nu n_e n_\nu \alpha_{e\nu}(\bar{T}e - \bar{T}\nu) \qquad (10)$$

$$- \sum_i \chi_{i,i+1}\left(n_e n_i \delta_{i,i+1} - n_e^2 n_{i+1}\delta_{i+1,i}\right) - S$$

Here σ is the electric conductivity

$$\sigma = \frac{3\sqrt{\pi}}{8\sqrt{2}} \frac{e^2}{\sqrt{m_e k T_e}} \frac{n_e}{\sum_\nu n_\nu Q_{e\nu}} \qquad (11)$$

$j = -\vec{n}_e e \vec{v}_e$ is the current density, s the radiation loss per cm^3 and $\chi_{i,i+1}$ the ionization energy.

The first term in (10) represents the Joule heat, the second the heat exchange between electrons and the other components of the plasma. The third term considers the reaction losses. In the case of the Saha-equilibrium it would disappear. The last term S is the radiation loss, which is calculated below.

Analogueus to (10) the collision integral for ions and atoms is

$$\left\{\frac{\partial}{\partial t}u_i\right\}_{coe} = n_e n_i \alpha_{ei}(\bar{T}_e - \bar{T}_i) + \sum_j n_\nu n_i \alpha_{ei}(T_\nu - T_i) \qquad (12)$$

The term which is analogue to j^2/σ is very small and neglected from the beginning. This means that in an electrical field primarily the electron component is heated. In thermal state the energy passes from the electrons to the other components. The second term means the possible energy exchange between heavy particles which practically can be neglected.

Now we calculate the emission of radiation S. The total energy which the electron gas transfers to the radiation field per s and cm^3 is

$$S(\vec{r},t) = \iint \left\{ \varepsilon_\nu(\vec{r},t) - \varkappa_\nu(\vec{r},t)\, I_\nu(\vec{r},\vec{\Omega},t) \right\} d\vec{\Omega}\, d\nu \qquad (13)$$

$$\vec{\Omega} = \vec{\Omega}(\vartheta,\varphi)$$

Here the emission coefficient ε_ν and the absorption coefficient $\varkappa_\nu$ are properties of matter at point $\vec{r}$ and time t, i.e. functions of the particle states. They depend on density, temperature and kind of plasma, while the radiation intensity $I_\nu = I_\nu(\vec{r},\vec{\Omega},t)$ results from the radiation transport equation (σ_ν = total scattering coefficient):

$$\vec{\Omega}\cdot\frac{\partial}{\partial\vec{r}} I_\nu(\vec{r},\vec{\Omega},t) = \varepsilon_\nu(\vec{r},t) + \sigma_\nu(\vec{r},t)\int I_\nu(\vec{r},\vec{\Omega}',t)\frac{d\vec{\Omega}'}{4\pi} \qquad (14)$$

$$-\left(\varkappa_\nu(\vec{r},t) + \sigma_\nu(\vec{r},t)\right) I_\nu(\vec{r},\vec{\Omega},t)$$

The scatterings $\vec{\Omega} \rightarrow \vec{\Omega}'$ are losses, while the scatterings $\vec{\Omega}' \rightarrow \vec{\Omega}$ means increases. Eq. (14) is especially of interest in astrophysics. Here it is only considered in plane geometry.

In general the calculation of the intensity gets very extensive. Therefore, we assume local radiation equilibrium, grey radiation and in addition neglect the scattering coefficient. In the case of an optically thin plasma it is possible to neglect absorption. Thus the radiation loss per cm and s results directly from the emission coefficient. Whether such a plasma is realized depends on the optical thickness of layer $\varkappa \cdot r_o$ which must be much smaller than unity (r_o = radius of plasma channel). Our nitrogen plasmas do not fulfill this condition, the hydrogen plasmas however do.

The equations (1 - 3) just discussed will now be applied to the heating experiment described in the following.

3. Impulse Discharge in Hydrogen.

3A. Electrical Data

For the heating of the plasma condenser banks are used, their data lying between the values given in table 1. The detailed experimental arrangement is described by Kluge-Höcker (1960).

Table 1.

Data of condenser banks

Capacity	c	= 7,7/uF	38,5/uF
Voltage	u	= 18 kV	
Maximum current	I_{max}	= 50 kA	120 kA
Current rise	dI/dt_{max}	= $1 \cdot 10^{10}$ A/s	$1,5 \cdot 10^{11}$ A/s
Rise time up to first current max.	t_A	= 1,5/us	4/us

Fig. 6 shows a characteristic current-voltage diagram of the impulse discharge. The heating process is finished before the current maximum is reached. In order to keep the influence of the mechanisms which transport the energy out of the plasma, as small as possible, the available energy must be pumped into the plasma very quickly. This requires highly developed short time measurements in connection with photography, spectroscopy and probe techniques.

Our short time equipment has been described in several publications in German: Maier and others (1960), Schneider and others (1961), Maisenhälder and others (1961).

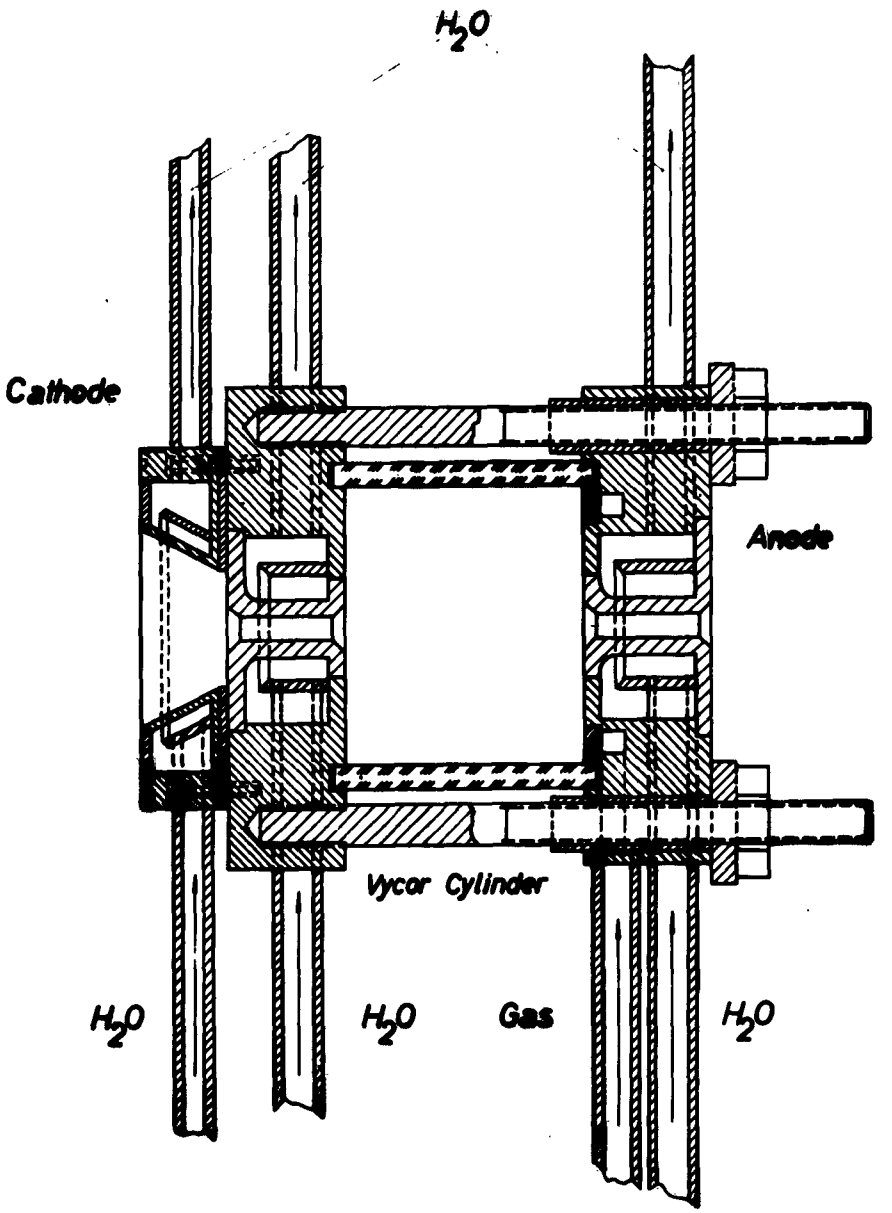

Fig 1 Discharge Chamber

Fig. 2 Whirl stabilized arc

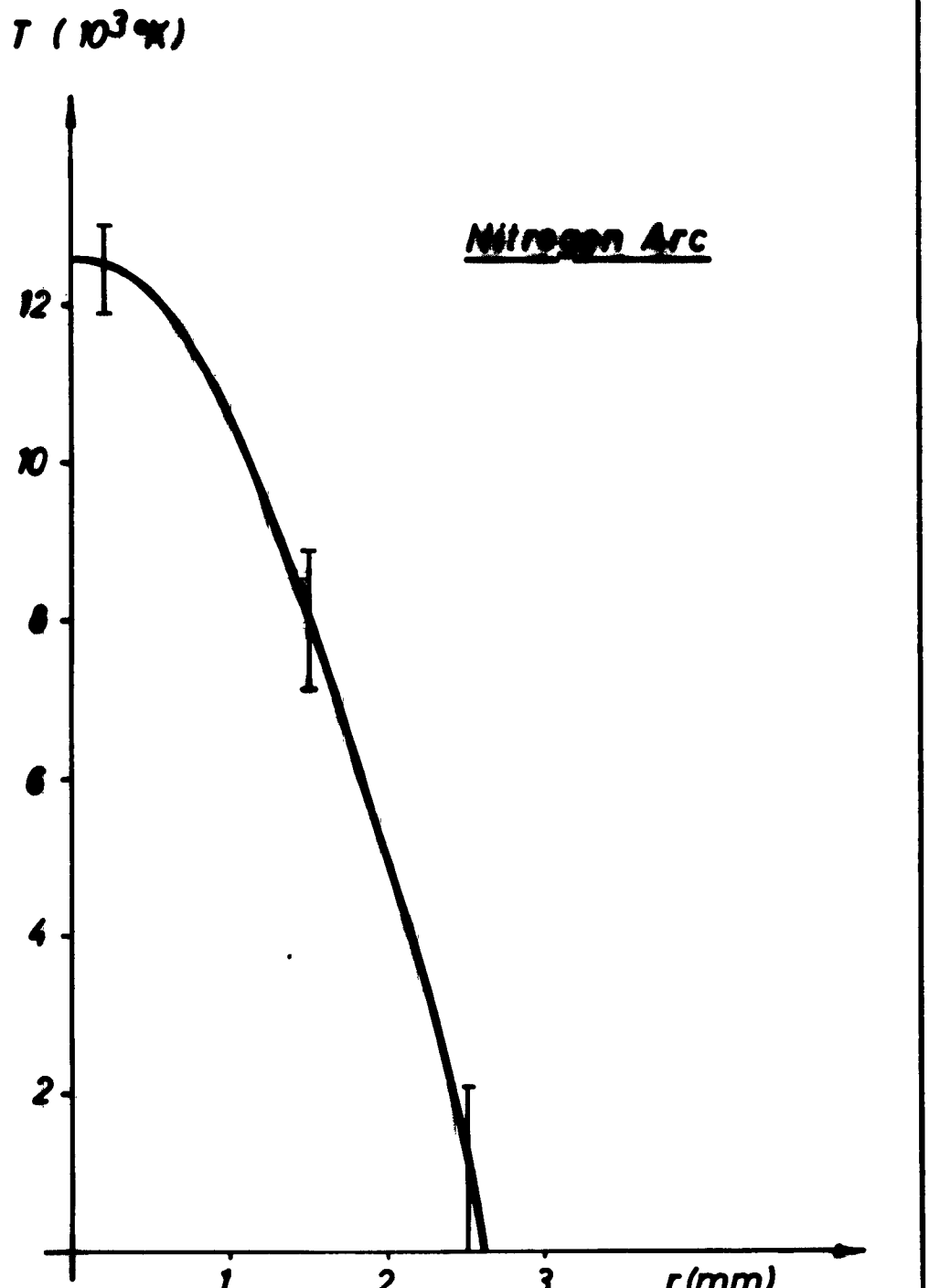

Fig. 3 Temperature Profile

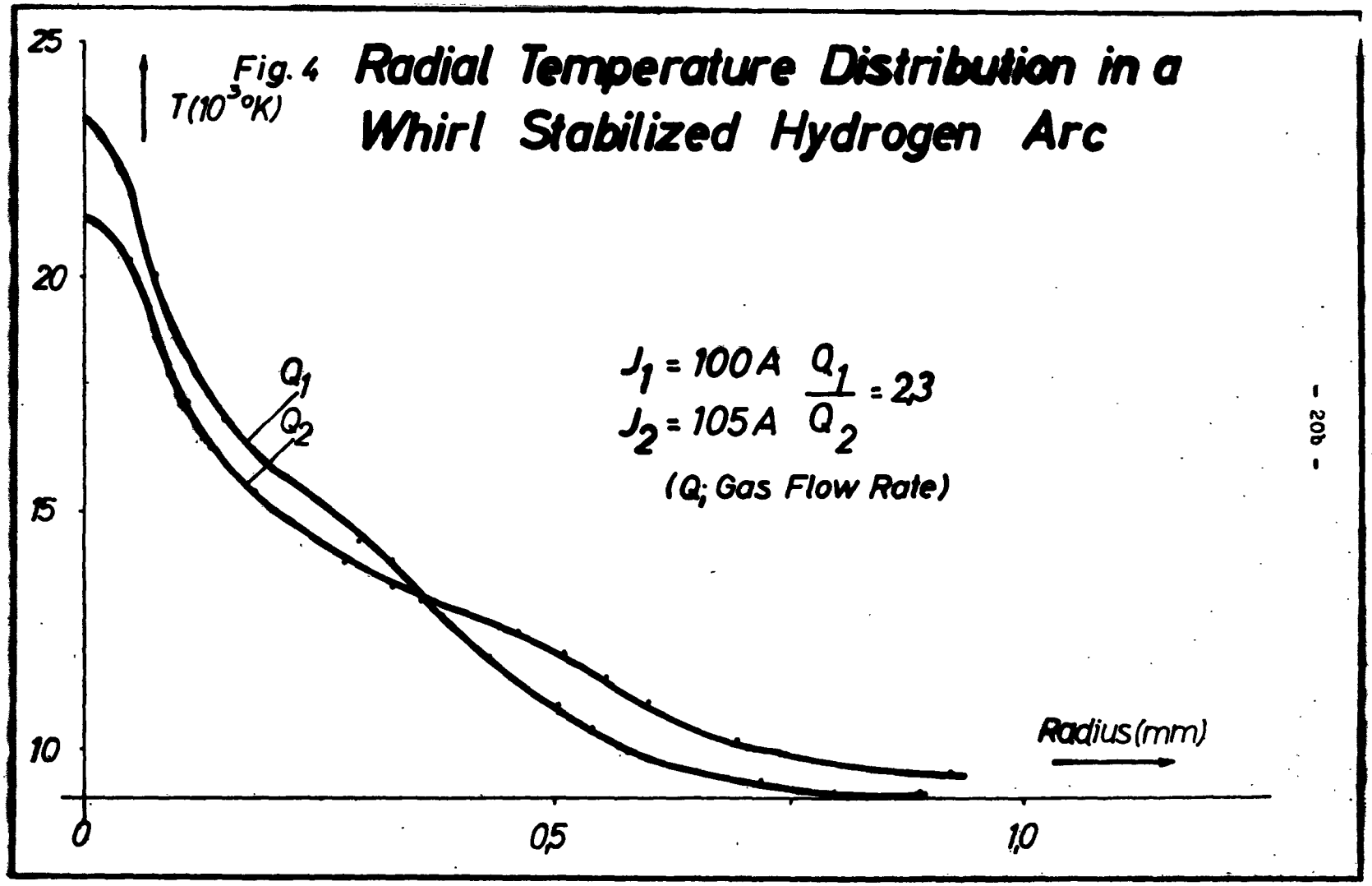
Fig. 4 Radial Temperature Distribution in a Whirl Stabilized Hydrogen Arc
T(10³°K)
25
20
15
10
0
0,5
1,0
Radius (mm)
Q1
Q2
J1 = 100A Q1/Q2 = 2,3
J2 = 105A
(Q: Gas Flow Rate)

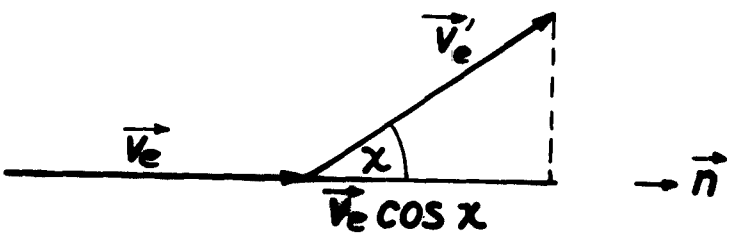

Fig. 5 Scattering of an Electron by a Heavy Particle. In the Case of an Elastic Collision $|\vec{v}_e| = |\vec{v}_e'|$ and therefore the Impuls in Direction of $\vec{n}$ after the Collision is Given by $\vec{v}_e \cos \chi$.

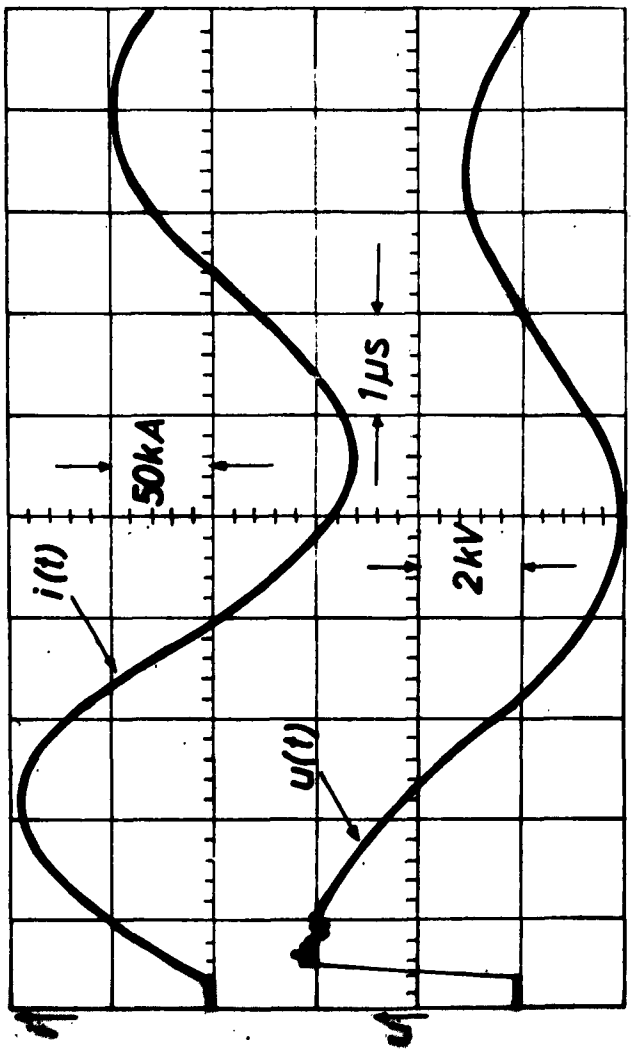

Fig6 Current and Voltage as a Function of Time

3B. Diagnostics with Magnetic Probes.

Image converter photographs indicated that the current transport takes place in a rather limited channel (Höcker-Kluge, 1959). The result was a high conductivity which, according to Spitzer, lead to rather high temperatures. This was rather unexpected and it seemed to be necessary to carry through other diagnostic investigation. Probe measurements promised to offer most information.

This method which has been developed and used for the investigation of low density plasmas, cannot be transferred without difficulties to dense plasmas. One complication is the thermal stress on the probe which is caused by the plasma. A probe arranged stationary in the discharge chamber is destroyed immediately by the stationary arc. Moreover, the geometry of the arc is considerably disturbed by flowing effects which cause an increase of pressure in front of the probe tip. Each of these two facts make it doubtful whether the method applicable for low density plasmas can be transferred to dense plasmas without modification.

In order to reduce the thermal stress on the probe, it may remain in the plasma only for a very short time. This condition was fulfilled by the following: an apparatus (see fig. 7) was constructed which shoots the probe into the discharge tube with a defined velocity, (about 1 m/s). At the same time, this method largely avoids the deflection of the plasma from its original position.

In order to be able to use the probe for several measurements, the discharge has to be switched off immediately after the phase which is of interest. If this is not done, the probe would be destroyed by the thermal stress of the stationary arc still existing after the transient discharge. The short-time cut-off of the arc is done by means of an electronic switch-off device. A suitable ignitron, which is in parallel to the discharge gap, is ignited at a definite moment and thus short-circuits the arc.

The magnetic probes (see Fig. 8) consist of copper wire (diameter 0,04 mm) which is wound on an insulating core with a diameter of 0,3 mm (16 windings). The coil is shorter than 1 mm. The supplies are twisted and shielded. The total length of the probe is about 77 mm. The noise could be kept down below noticeable values. The frequency characteristic is linear up to at least 17 M.c, the resonance frequency is 35 M.c.

These measurements show the probably simplest but most effective application of the probe method. The magnetic probe is being shot into the discharge tube perpendicular to its axis. The coil measures the change of the $\vec{B}_\varphi$ field generated by the current itself as a function of time. The discharge is ignited several times and the voltage signal of the probe is taken from the screen of a oscillograph. According to the induction law the oscillogram obtained yields the $\partial \vec{B}/\partial t$ variation at the point where the probe is located.

Then the probe is brought to another (radial) point and the process repeated, until there exist complete curves for the $\partial \vec{B}_\Theta / \partial t$ fields between wall and axis. After integration, curves $B_\Theta(r)$ can be constructed. The further application of these $B_\Theta(r)$ curves for the determination of currents and current densities is based on the assumption that the field distribution is cylinder-symmetric. The correctness of this assumption was confirmed by means of several probes with different orientation.

Using the mentioned symmetry condition, the first Maxwell equation yields by differentiation:

$$j_z = \frac{1}{\mu_0 r} \frac{\partial}{\partial r} (r B_\Theta) \qquad (15)$$

where j_z = current density parallel to the axis of the discharge tube (z-direction).

The electric field strength in z-direction, depending on the Ohmic resistance which is of interest for our investigations, is obtainable from the second Maxwell equation, provided that $\partial E_z / \partial z = 0$ along the axis of the discharge tube and that the Ohmic resistance of the leads can be neglected.

$$E_z = \frac{U_{tot}}{l} - \frac{\partial}{\partial t} \int_R^{R_0} B_\Theta \, dr \qquad (16)$$

(l = length of the axis, U_{tot} = total voltage between the electrodes, R_0 = distance between the return leads and the chamber axis).

The second term on the right hand side of the last equation represents the inductive part of the total voltage between the electrodes which was measured by means of coil probes. The determination of this term is also possible by means of loop probe measurements. The results obtained are given in fig. 9 and 10. Fig. 11 shows the variation of the first halfwave of the current $I_R(t)$ with the radius as parameter. R means the distance between the axis of the discharge tube and the probe. The outer curve gives the total current I_{tot} which was measured by means of a Rogowski coil. The behavior of the plasma channel during the impulse discharge is demonstrated by the variation of the current curves. If the current is increased, the conducting channel which was created by the pre-discharge, is expanded to the range of larger diameters. This corresponds to the visible expansion of the luminous plasma zone. The curves for $R = 6 - 15$ mm show the same variation. Therefore, it is obvious that during the first halfwave of the current the channel is only expanded to a radius of 6 mm. On page 66 ff. will be shown that the expansion is due to an ionization of the outer zone effected by the radiation of the core of the discharge. The current density is obtained by graphic differentiation of the $I_R(t)$-curve.

$$j_t(R) = \frac{\partial J_z(R)}{\partial F} = \frac{1}{2\pi R} \quad \frac{\partial J_t(R)}{\partial R} \qquad (17)$$

Fig. 9 shows the results for times $t < 2 \cdot 10^{-6}$ s and $2{,}5 \cdot 10^{-6}$ s $< t < 4 \cdot 10^{-6}$ s; fig. 10 gives the results for times $t > 5 \cdot 10^{-6}$ s. The curves in fig. 9 mainly represent

the current density distribution for the case of increasing currents, in fig. 10 for the case of decreasing currents beyond the first current maximum. It is obvious that there exists a narrow zone with high current density and low current and a larger zone with low current density and higher current. Our earlier image converter photographs did not show these results. At early times ($t \leq 0{,}5 \cdot 10^{-6}$ s) the current density shows a variation which could be expected from the geometry and the conductivity profile of the pre-discharge. Later the current density decreases less steep, e.g. the plasma expands in direction of the radius. Since this area includes the optically visible contact zone between plasma and outer gas, it seems reasonable to attribute these occurences to the mentioned expansion mechanism.

Fig. 12 shows the Ohmic part of the electric field strength which was determined by means of coil probe measurements, and fig. 13 the conductivity resulting from current density and E_z-field strength according to the Ohmic law. The curves $E_z(t)$ are equal to zero close to the times $5{,}6{,}7 \cdot 10^{-6}$ s. Therefore, the calculations for these times are rather uncertain, and the representation of the curves for the mentioned times was dropped. For the temperature estimation the relation between conductivity and temperature, given by Schrade (1961) was used. The results are represented in fig.14. As the E_z curves near the times $12 \cdot 10^{-6}$ s and $14 \cdot 10^{-6}$ s are equal to zero too, the temperatures for these times neither correspond to the actual physical facts. A more comprehensive description of method and results of probe measurements is given by Thiele (technical note of contract AF 61 (052)-590) (1963).

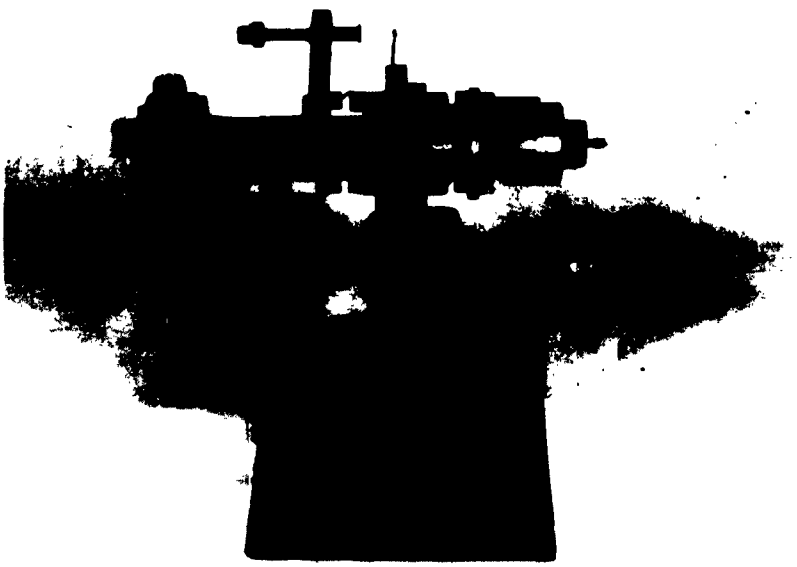

Fig. 7 Probe Gun

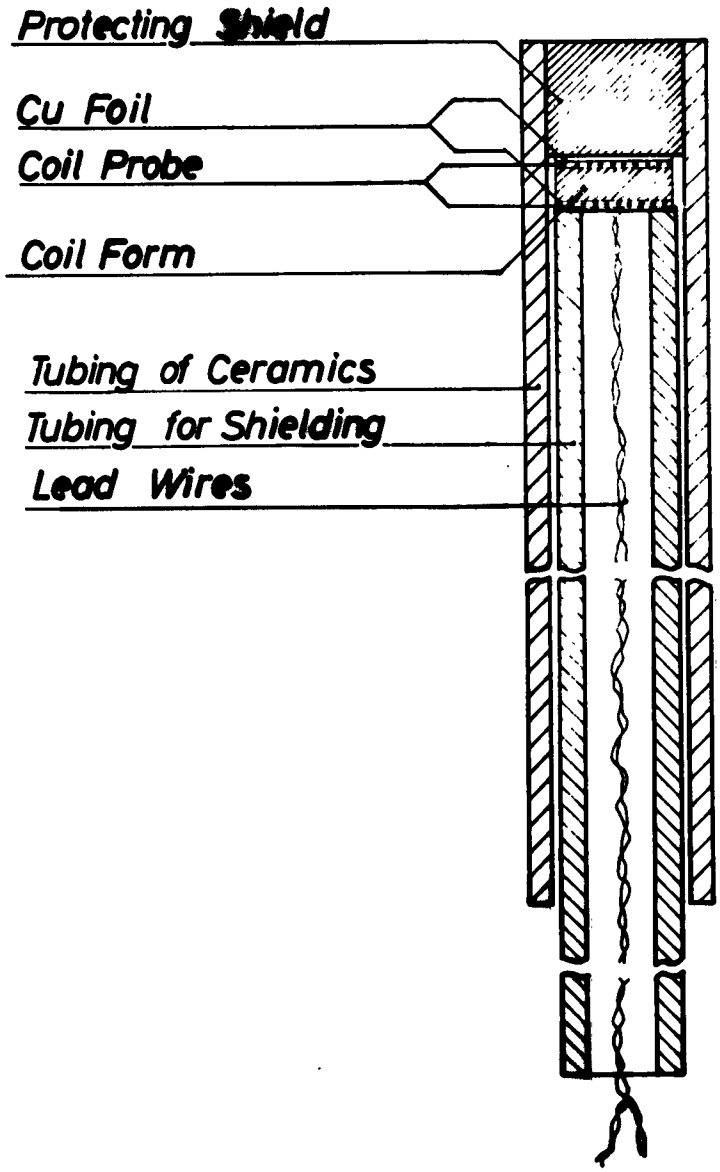

Fig. 8 Magnetic Probe

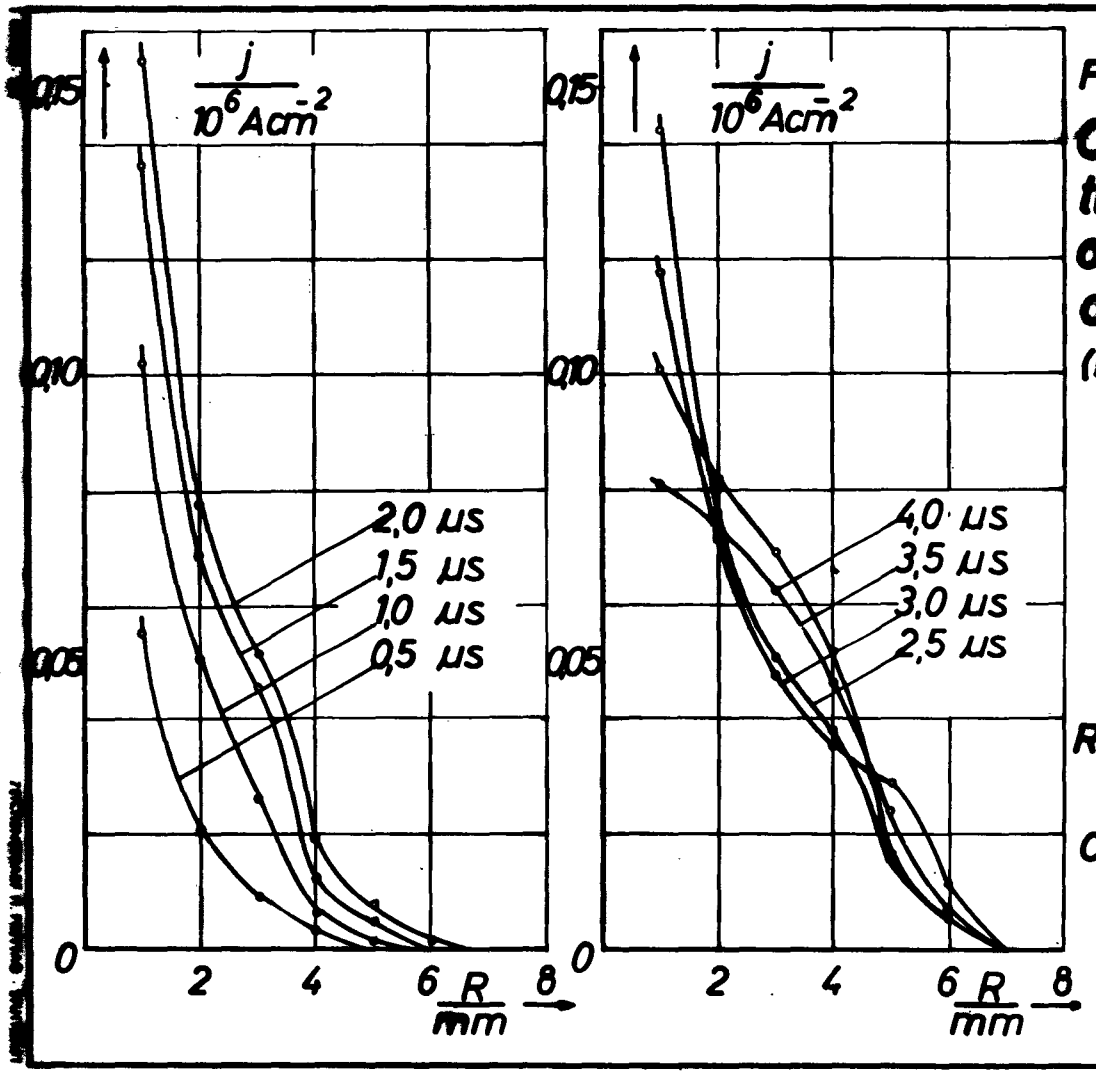

Fig.9

Current Density Distribution as a Function of Radius with Time as a Parameter

(Magnetic Probe Measurements)

Radius of the stationary Arc

$R \approx 2{,}5\,mm$

Current Density of the stationary Arc

$j_{Arc} = 0{,}0005\ 10^6\,Acm^{-2}$

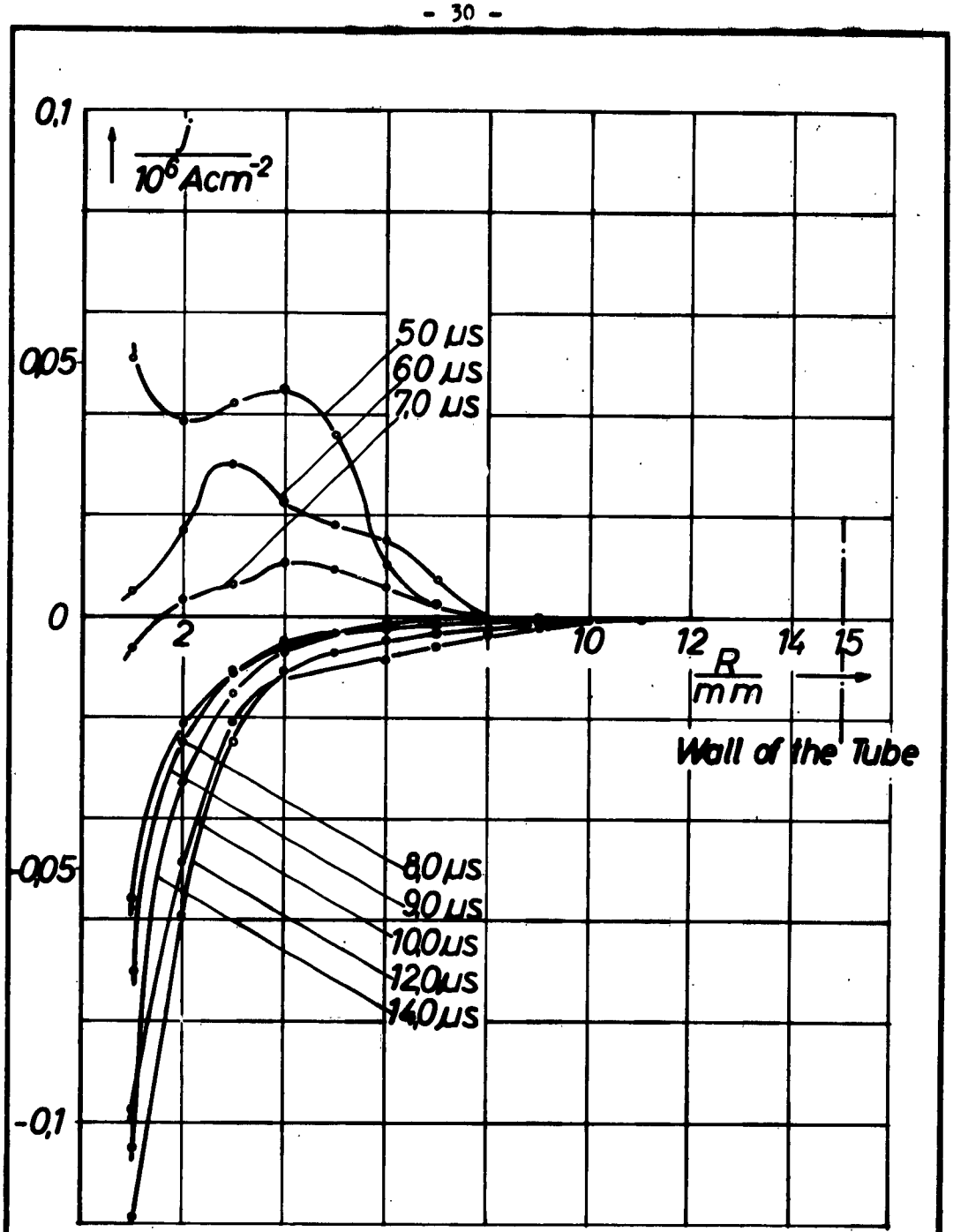

Fig. 10 Current Density Distribution as a Function of Radius with Time as a Parameter
(Magnetic Probe Measurements)

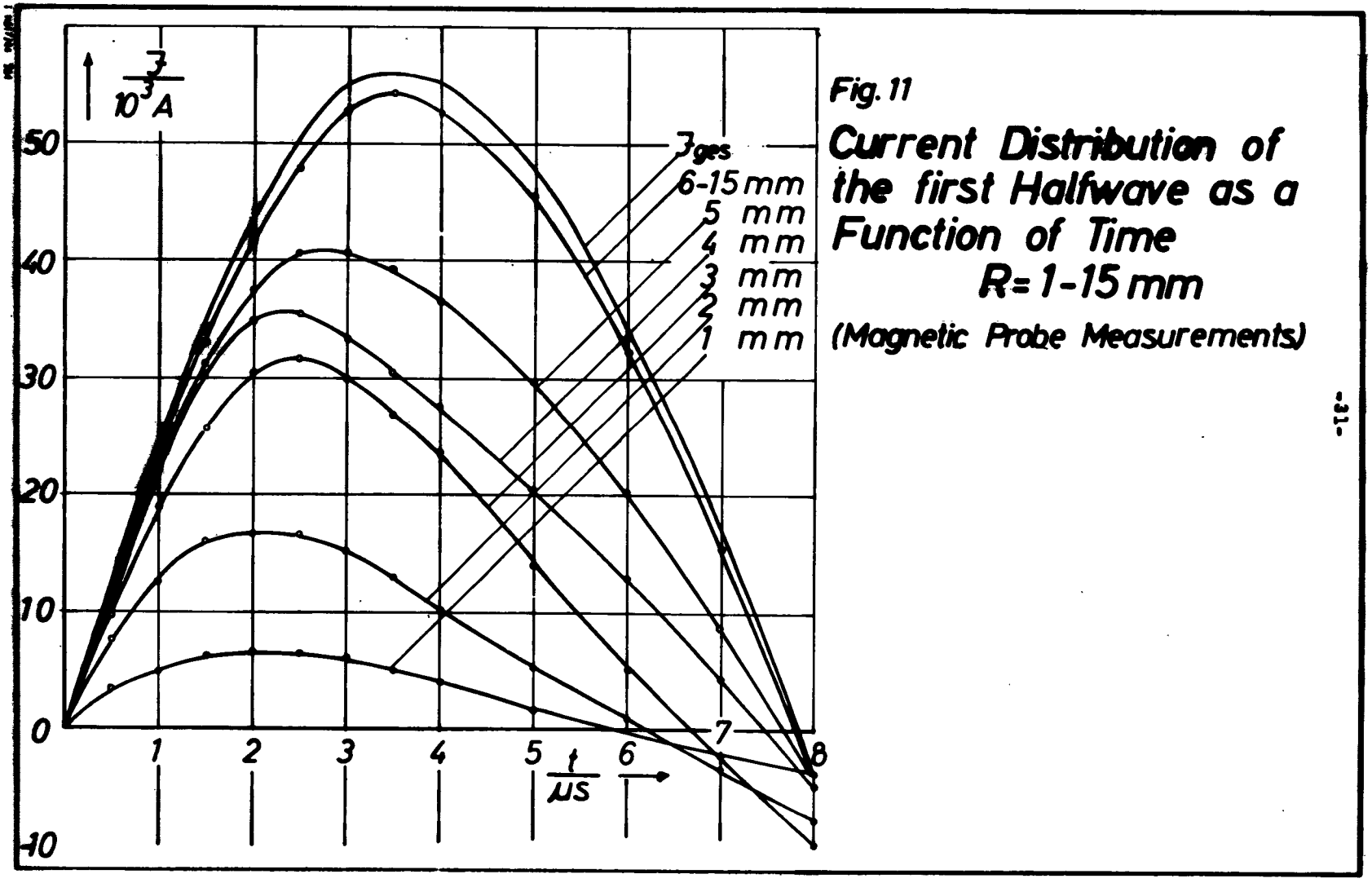

Fig. 11

Current Distribution of the first Halfwave as a Function of Time

R = 1-15 mm

(Magnetic Probe Measurements)

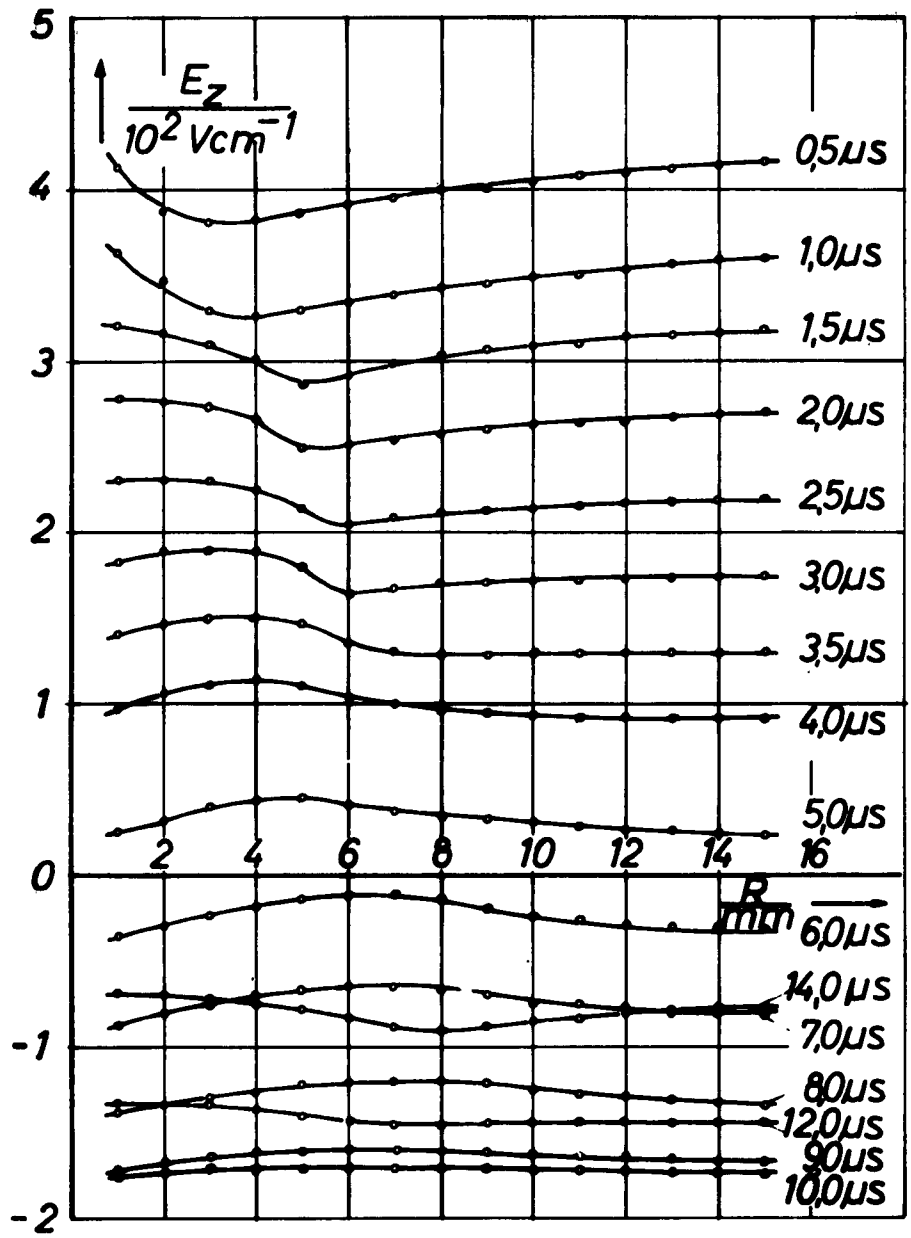

Fig.12 *Ohmic Portion of E_z Field Strength as a Function of the Radius with Time as a Parameter*

(Magnetic Probe Measurements)

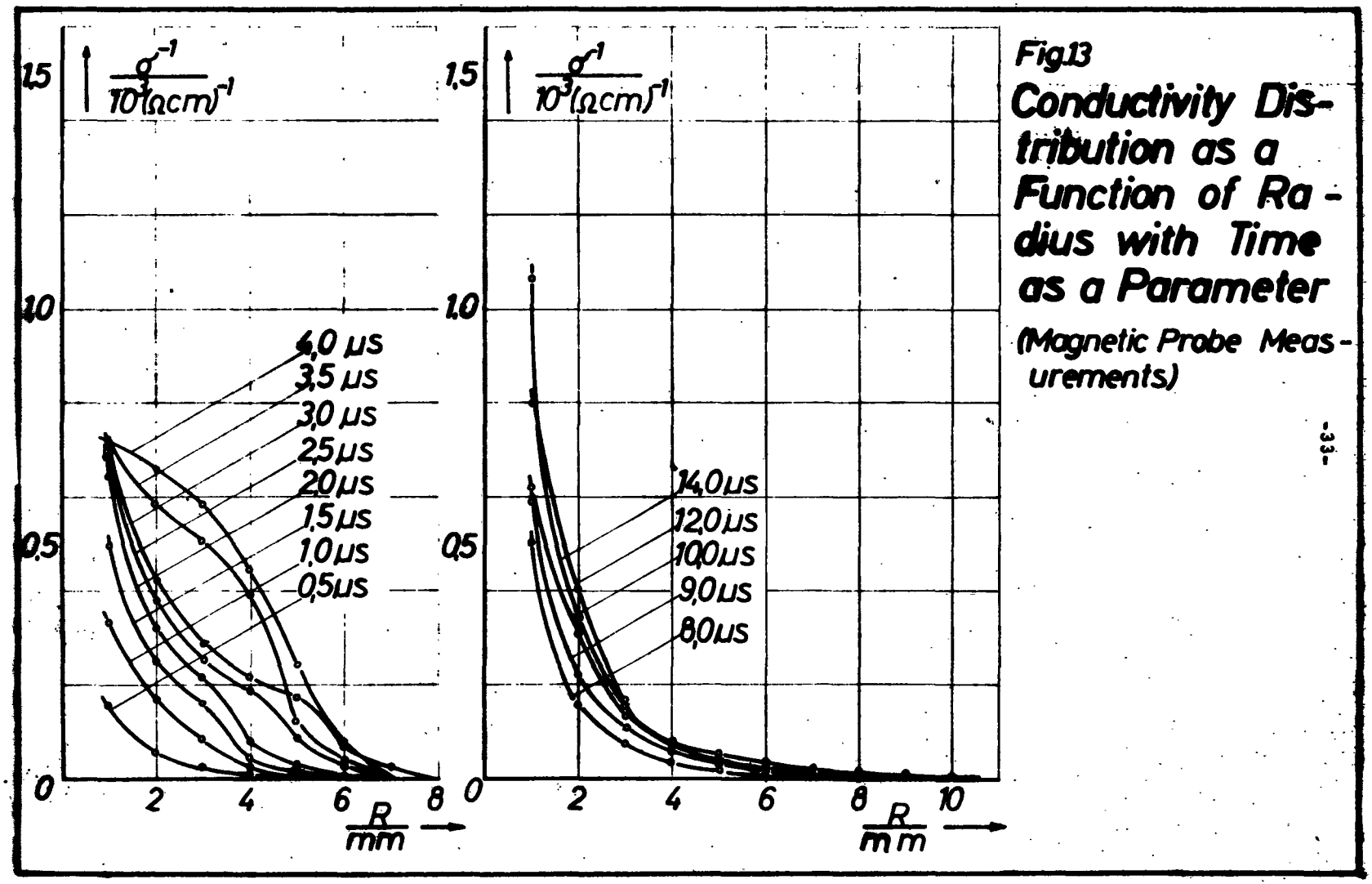

Fig.13

Conductivity Distribution as a Function of Radius with Time as a Parameter

(Magnetic Probe Measurements)

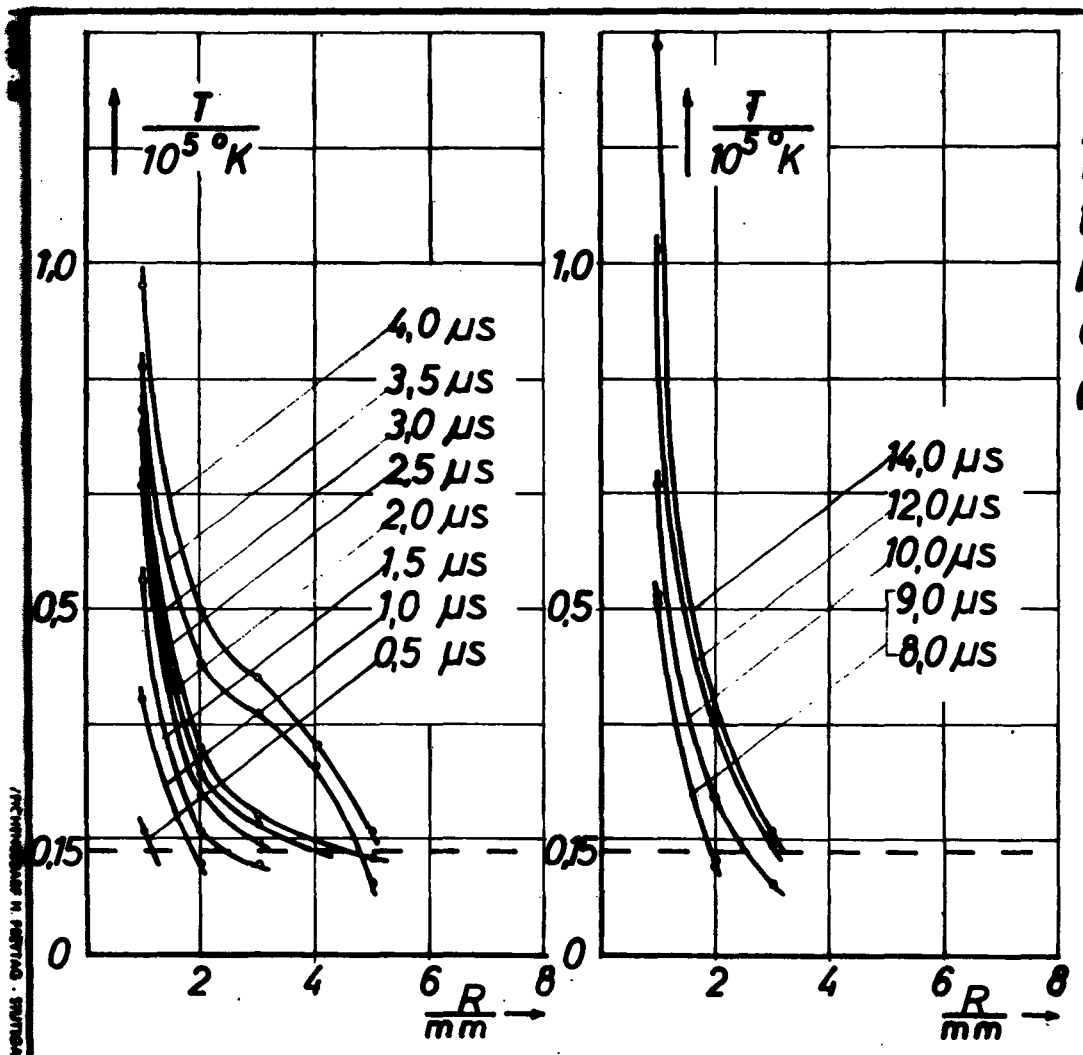

Fig.14

Temperature Distribution as a Function of Radius with Time as a Parameter

(Magnetic Probe Measurements)

3C. Diagnostics by Means of Spectroscopic Measurements.

a) Apparatus.

For the spectroscopic measurements two prism spectrographs were used, a Fuess 110 M with a natural quartz prism and a Zeiss-3-prisms spectrograph with glass prisms. The main part of the investigations was carried out with the Fuess 110 M (Fig. 15). Its dispersion reaches from 5 Å/mm at 2000 Å up to 50 Å at 5 000 Å (Fig. 16) and the resolving power from 10^5 at 2000 Å to $4 \cdot 10^3$ at 5 000 Å (Fig. 17). The spectra were enlarged (20 times) by means of a projector and then measured. Assuming that the error of the measurement is 1/5th mm, the error in the wavelength of a spectral line near 2 000 Å is about 0,05 Å and near 5 000 Å about 0,5 Å.

The natural quartz prism has a basic length of 80 mm and is 42 mm high. The focal length of the collimator lens (quartz) is 585 mm, its diameter 52 mm. The data for the camera lens are: focal length 635 mm, diameter 64 mm. The aperture ratio is 1 : 11 and the length of the spectrum 225 mm. By means of a micrometer screw the entrance slit can be adjusted to a width of 1/10 µ. By means of Hartmann diaphragms the height can be regulated from 1 to 10 mm. The diaphragma makes it possible to produce 10 different spectra, each 1 mm high. As spectral plates "Perutz 450 spectral-blue" were used. The size of the plates is 27 x 6 cm.

Fig. 18 shows the path of light of the Zeiss-3-prism spectrograph. Some of its data are:

Spectral range:	3 600 to 10 000 Å
3 glass prisms:	210 mm basic length, 54 mm height
Collimator lens:	300 mm focal length, 60 mm diameter
Camera lens:	270 mm focal length, 60 mm diameter
Aperture ratio:	1 : 5,5
Length of spectra:	80 mm
Size of plates:	6 x 9 cm

b) Imaging and Adjustment Methods

For the structure analysis the discharge channel was imaged on the entrance slit of the spectrograph. Fig. 19 shows the corresponding path of light.

The reference spectra were obtained from high voltage sparks between the electrodes of Al, Cu, Zn and W. The calibration was done with the aid of an iron spectrum. Fig. 20 shows the path of light for such reference spectra. The aluminium mirror can easily be replaced, thus the adjustment of the lenses for the photograph of the discharge is retained.

For the structure analysis of the arc several kinds of imaging can be used. They are shown in Fig. 21. Most of the spectra were photographed side-on-across, since the diameter of the discharge first plays an important part. The exposure time was regulated by means of a shutter (1/500 to 1 s). It was opened manually in the case of the

stationary arc and in the case of the impulse discharge by means of an electric contact coupled with the ignition device. We succeeded in resolving the impulse discharge in so much as necessary by means of the mechanic shutter described in the following paragraph. The image of the discharge on the slit of the spectrograph was photographed at the same time when the spectral plate was being exposed. This provided an information about that part of the discharge that actually delivered the light for the spectral apparatus.

e) Shutter for Short-time Spectroscopy

For the time-dependent resolution of the light emitted by the impulse discharge, very short times are necessary. The current rise time of the fastest impulse used here was 1,5/us; as will be seen later, the maximum temperature is reached at 0,6/us after ignition. Therefore, for the time-dependent resolution of this process opening times in the range of 10^{-7} s are required.

In 1960, R. Schneider and M. Mailänder have described a shutter for short exposure times. Its principle is given in the following (fig. 22): The shutter has two discs, one running with maximum 20 000 revolutions per minute, the other is set in motion in order to open the shutter. It is stopped after approximately half a revolution. Both discs have slits. The slit of the first disc is 20/u broad. The slit of the other one can be changed in such a way that during its opening time the running disc performs

just one revolution. This guarantees only one single exposure.

The slit of the first disc is imaged on the spectrograph slit by means of the achromate A_1. The opening time of the shutter amounts for one point of the spectrograph slit with a distance h from the optical axis to:

$$t = \frac{60}{2\,n} \cdot \frac{a d_1 + d_2}{a r_m + h} \qquad (18)$$

where n = number of revolutions of the first disc (U/min)

a = imaging ratio

r_m = distance: axis of the revolving disc - optical axis

d_1 = Breadth of the revolving slit

d_2 = Breadth of the spectrograph slit

The ignition of the discharge has to be done at a defined moment before opening the shutter. This may be done by means of a path of light according to the dotted line in fig. 23. The illuminated slit S_1 is imaged by means of the mirror Sp_2 on the slit of a photomultiplier. This path of light is adjusted in such a way that the photomultiplier receives a light impulse shortly before the slit S_1 passes the optical axis and by this exposes the spectrograph. If the revolution frequency of the revolving disc is constant, the electric signal coming from the photomultiplier lies a distinct time before the moment of the exposure.

The signal coming from the multiplier M_1 (fig. 23) is amplified by the amplifier V_1 and switches the ignition device on. The retarder R allows the regulation of the

ignition moment.

In order to obtain time marks for the photomultiplier impulse, the spark and the exposure time, the photomultiplier M_2 and the oscillograph are synchronized. The slit of the revolving disc is illuminated by means of the lamp L_2 and the light passing through the spectral apparatus reaches the multiplier M_2. The voltage signal is given to the oscillograph after amplification in the amplifier V_2. The oscillograph is triggered by the signal from the Multiplier M_2. By pick-up of the signal from the ignition device, the ignition spark is written on the oscillograph as well. On the screen appear therefore the signals sketched in the figure. By means of the retarder the ignition spark can be moved to any point of time. The zero adjustment of the retarder is given by the point of time when ignition impulse and exposure time coincide.

The exactness of the triggering is better than 10^{-7} s. The reproducibility of the moment chosen is also 10^{-7} s. This was controlled by means of the multiplier M_2 before and after the exposure of the plate.

Oscillations of the revolving disc, which would cause an increase of the exposure time, could not be observed. Oscillations in direction of the disc axis are avoided by a special form of the disc. Oscillations in radial direction are being compensated, since the same slit is used for trigger impulse and exposure impulse.

A possible deformation of the slit caused by the centrifugal force due to the high revolution frequency was not observed. The exposure signal of the multiplier M_2 which was obtained for high and low revolution frequencies had always the same shape.

The spectra were taken on Kodak I-O-plates.

d) Results of the Short-time Spectroscopy with a Slow Impulse

The series of spectra shown in fig. 24 was produced with the aid of the shutter for short exposure times. The current rise time of this discharge was 25 µs, the exposure time in each case 0,1 µs. The "slow" impulse was used as it allows an easier observation of the time-dependent variation of the spectral lines.

For several lines this variation can be clearly recognized. In fig. 24 (after 2,5 µs) practically only N I - lines are observable which become longer with time; this indicates the expansion of the discharge. In the second spectrum N II-lines appear and also, very weakly, N III-lines which become stronger with time. 11 µs after ignition the maximum temperature is reached. From then on the intensity of the N III - lines decreases again and after 25 µs they disappear completely. From the time integral spectrum (1/300 s) we gather that the main intensity is due to the N II - lines and partly also to copper lines. In comparison, the N III - lines which are visible for a short time, are suppressed.

e) Comparison to results with a "fast" impulse.

Fig. 25 shows a comparison of the spectra at the moment of

maximum temperature of the discharge of 1,5 /us rise time and 100 kA maximum current and a discharge of 25 /us rise time and 50 kA maximum current. In the spectrum of the fast discharge (fig. 25a) one clearly recognizes various zones: the hot core, which is indicated by the N IV - lines, then, surrounding it, a shell with predominant emission of N III - lines which, for their part, are surrounded by a shell of predominant N II - emission. The slow discharge (fig. 25 b) does not reach the high temperature; therefore, no N IV - lines are to be seen. The core emits only weak N III - lines, the main intensity, however, lies in the N II - lines. This is dealt with more comprehensively by Schneider (1961).

From this structure of the discharge channel a temperature profile can be calculated. The intensity of a spectral line is given by:

$$I = \text{const. } N\, e^{-E/kT}$$

with N = particle density and

E = excitation energy.

N may be taken from publications already known such as for instance W. Finkelnburg and H. Mäcker (1956) or W. Zimmermann and H.J. Kaeppeler (1961) and one obtains the relative intensity variation dependent on the temperature. This was done for the following three lines: N II = 3995 Å, N III = 4097 Å and N IV = 40 58 Å; the curves which are normalized for maximum intensity are represented in fig. 26. On the side of the low temperatures the curves decrease rapidly. If one assumes that a spectral line disappears if the intensity is reduced by a factor of 100, there results only a

small uncertainty in the temperature due to the mentioned high slope. The temperature profile of the impulse of 1,5 /us rise time at the moment of maximum temperature (0,6 /us after ignition) is represented in fig.27. The limits of error are given by the vertical strokes. By means of extrapolation one obtains an axis temperature of about 65 000 ^{o}K.

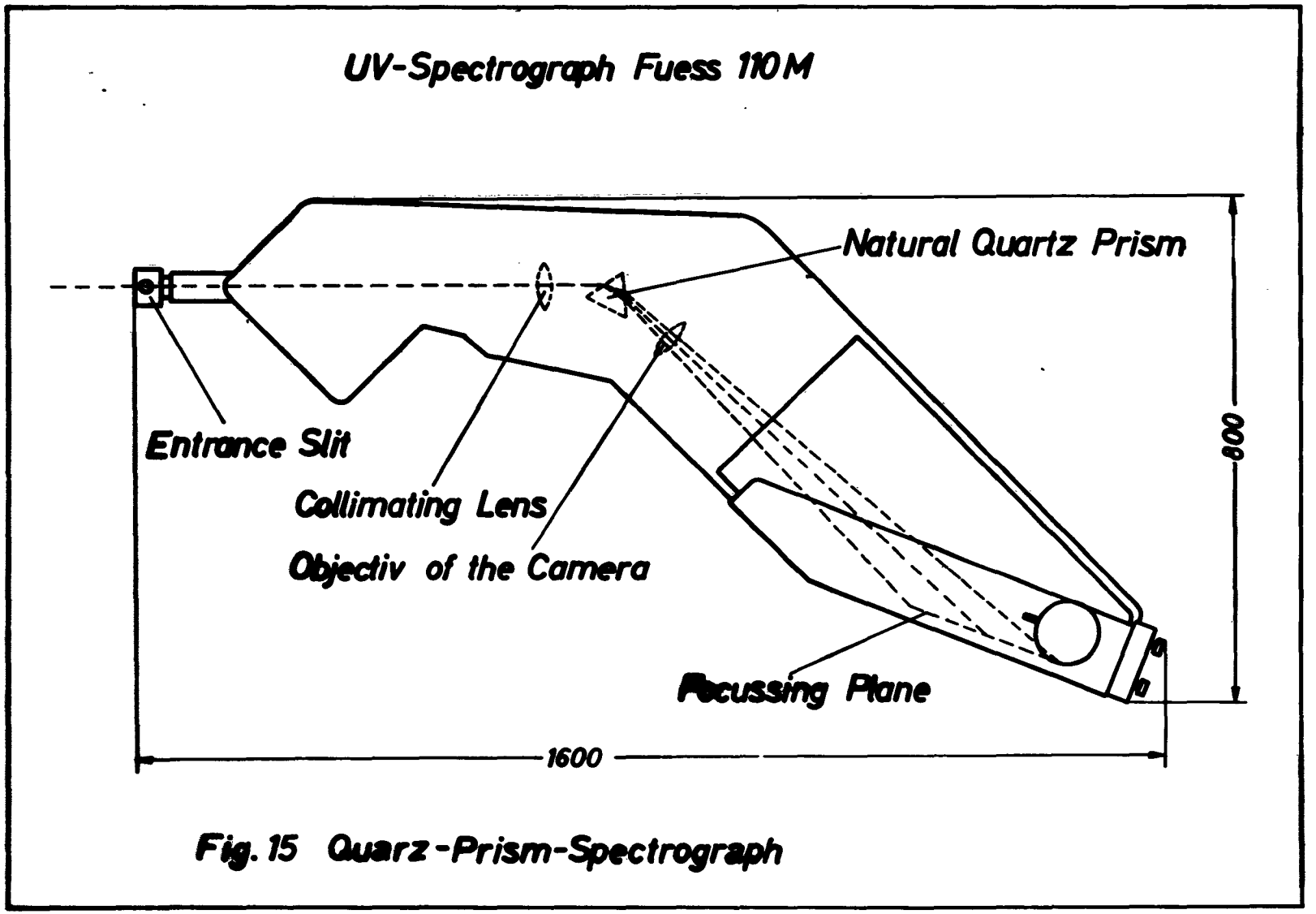

Fig. 15 Quarz-Prism-Spectrograph

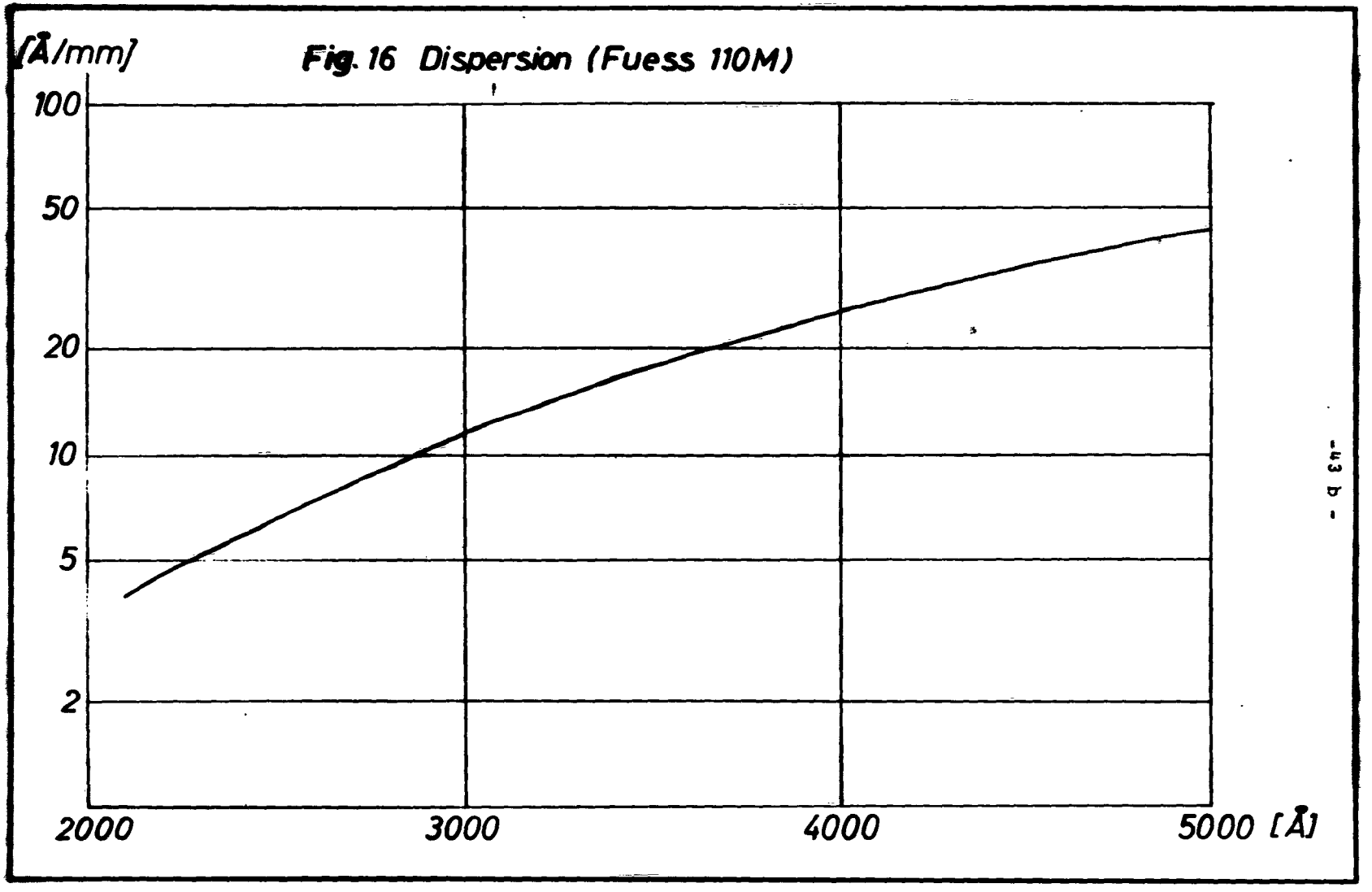

Fig. 16 Dispersion (Fuess 110M)

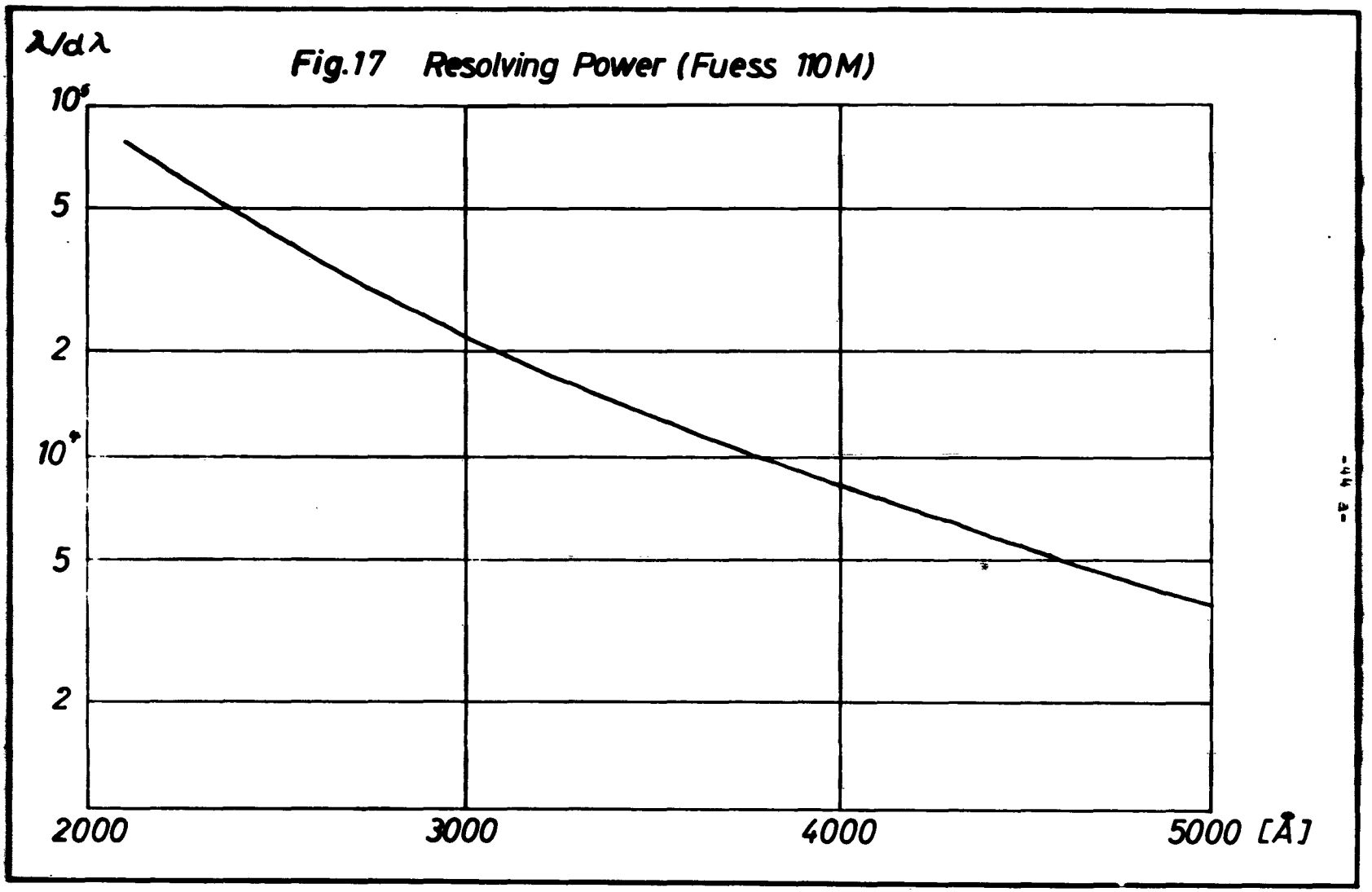
λ/dλ
Fig.17 Resolving Power (Fuess 110M)
10⁶
5
2
10⁵
5
2
2000
3000
4000
5000 [Å]

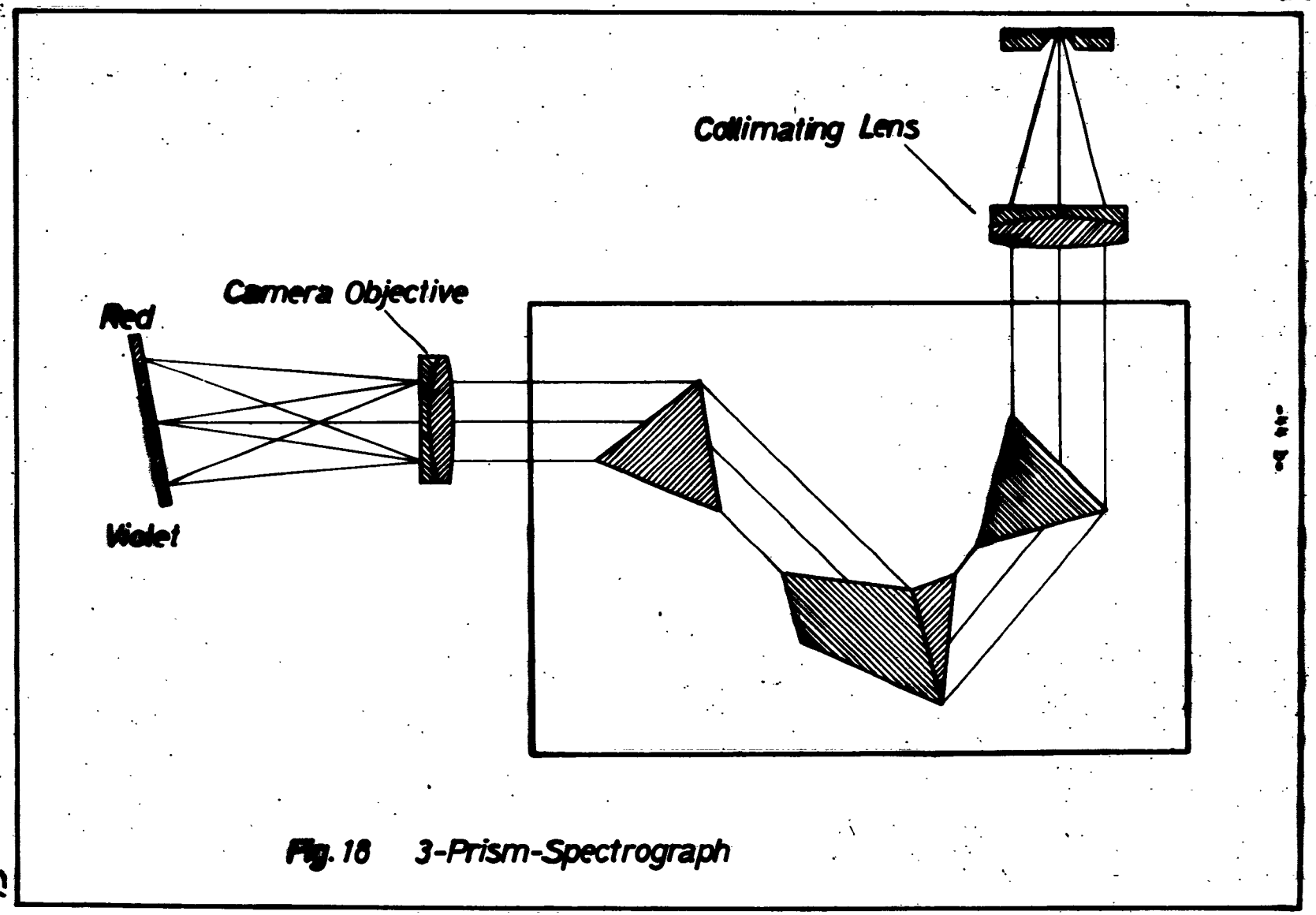

Fig. 18 3-Prism-Spectrograph

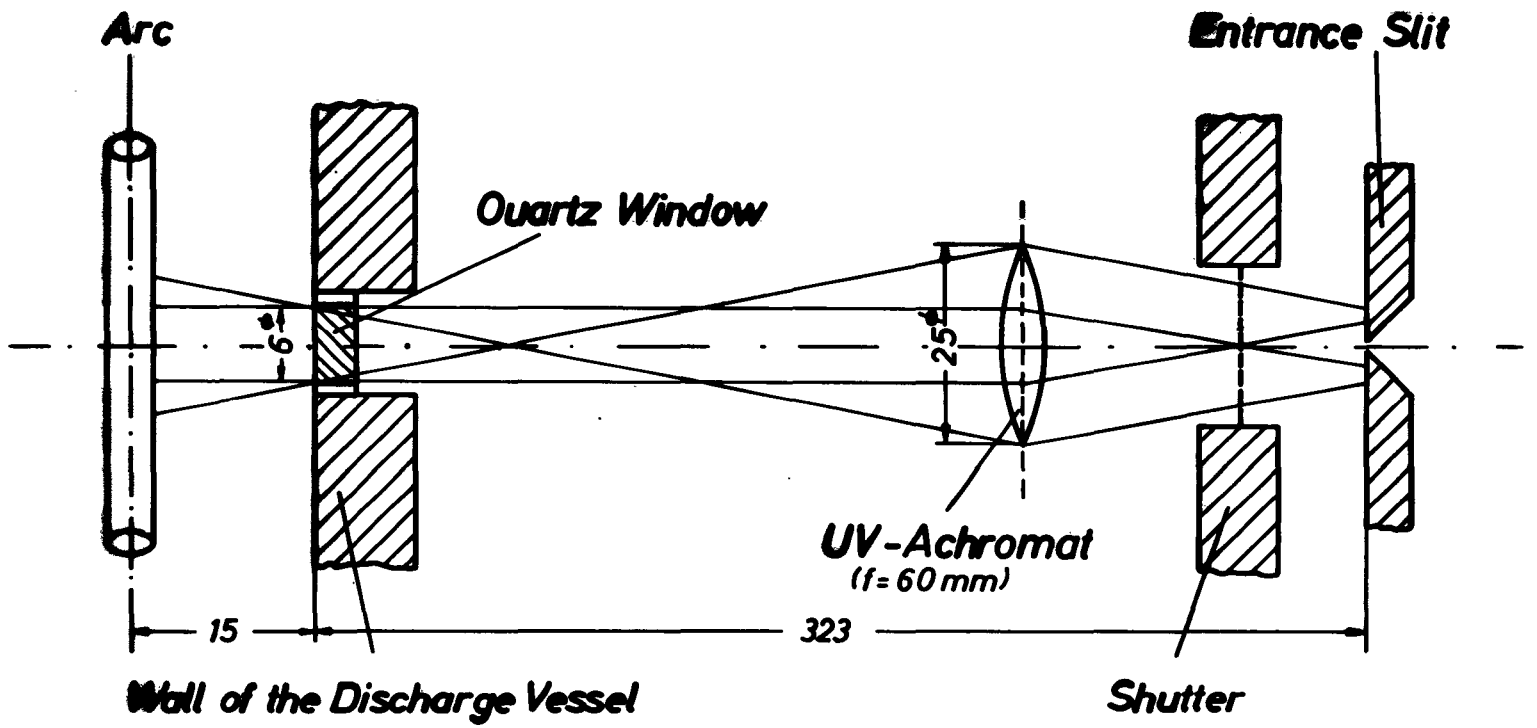

Fig. 19 Imaging on the Entrance Slit

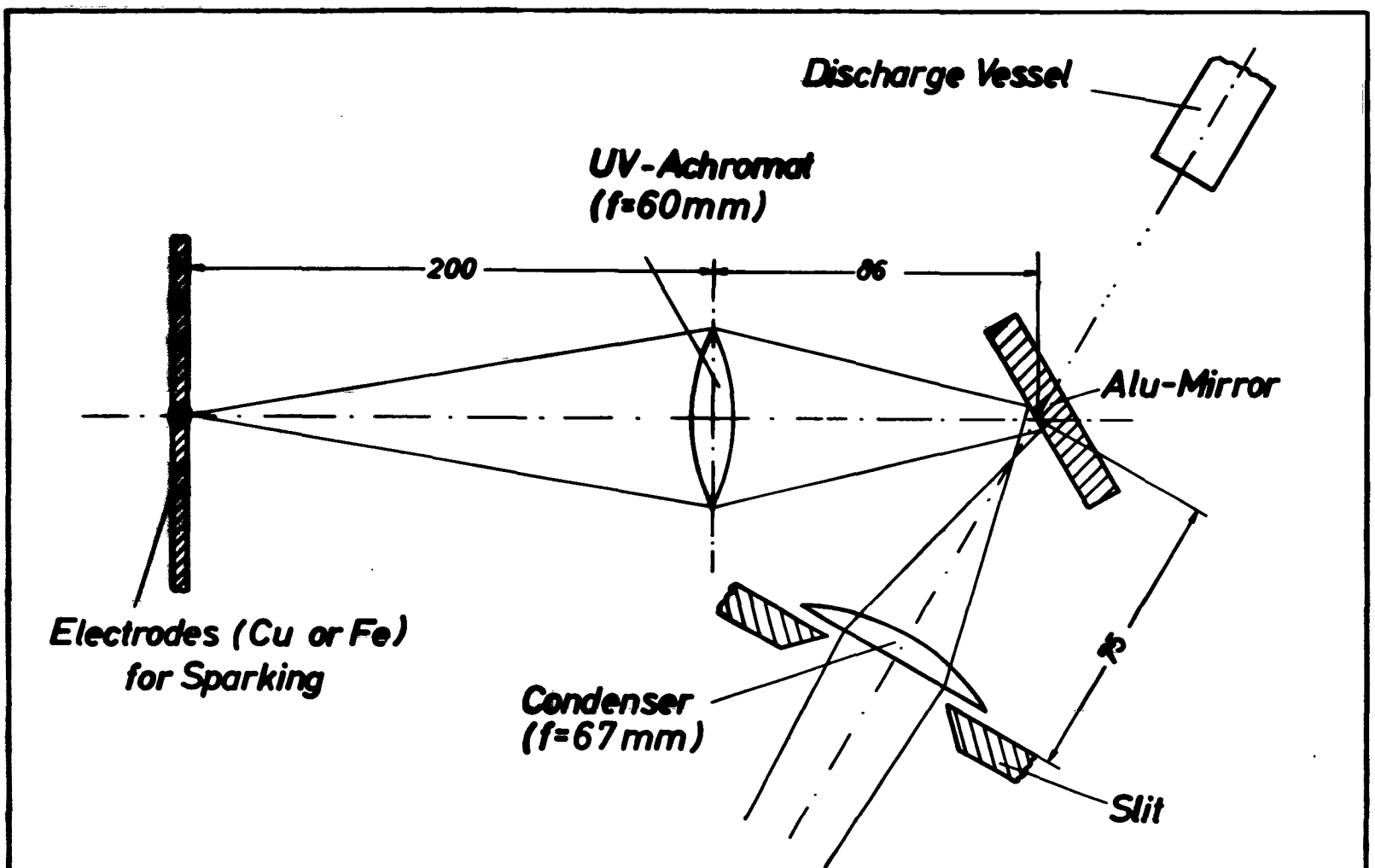

Fig. 20 Imaging on Collimating Lens

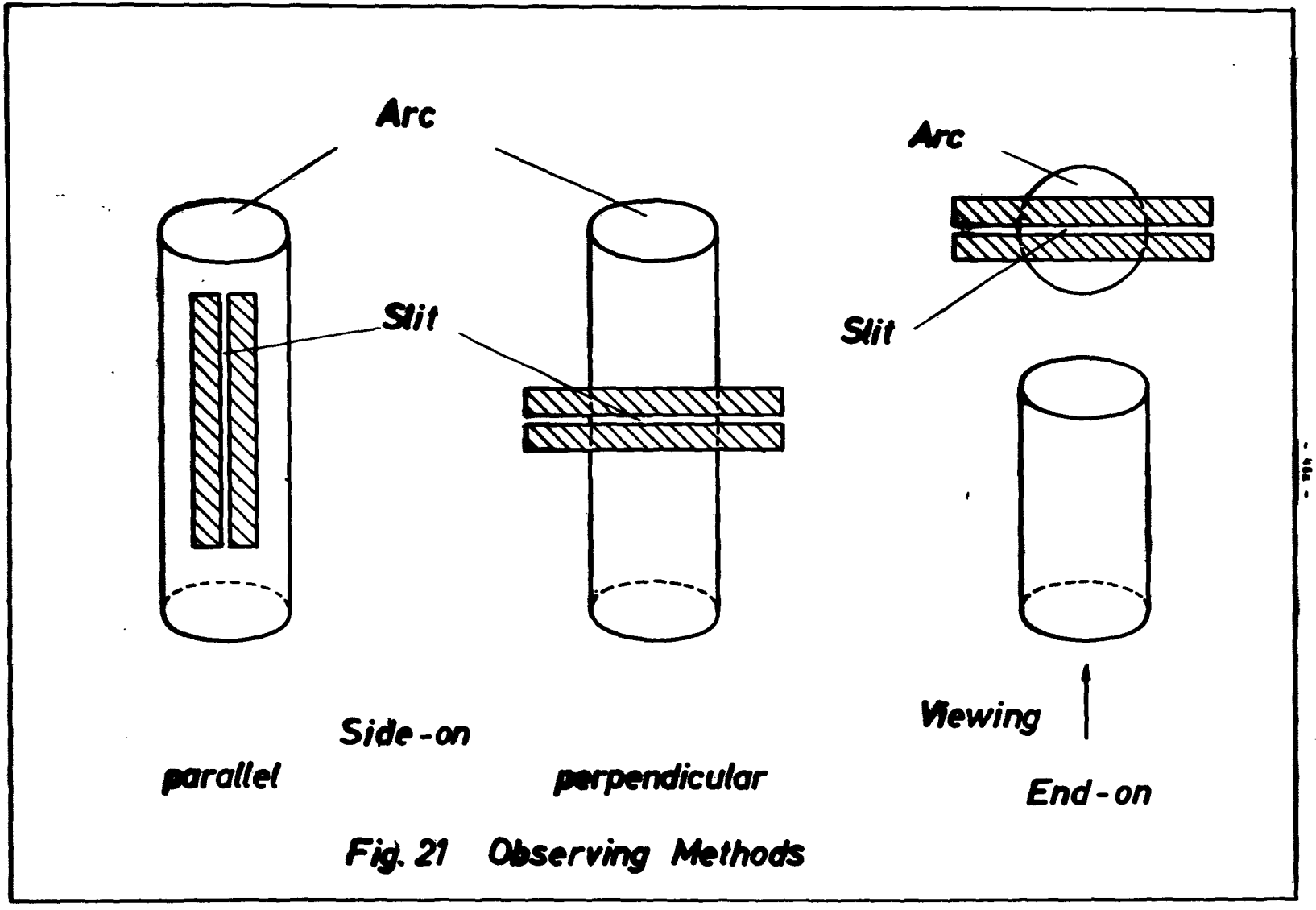

Fig. 21 Observing Methods

Fig. 22 Short-time Shutter (schematic)

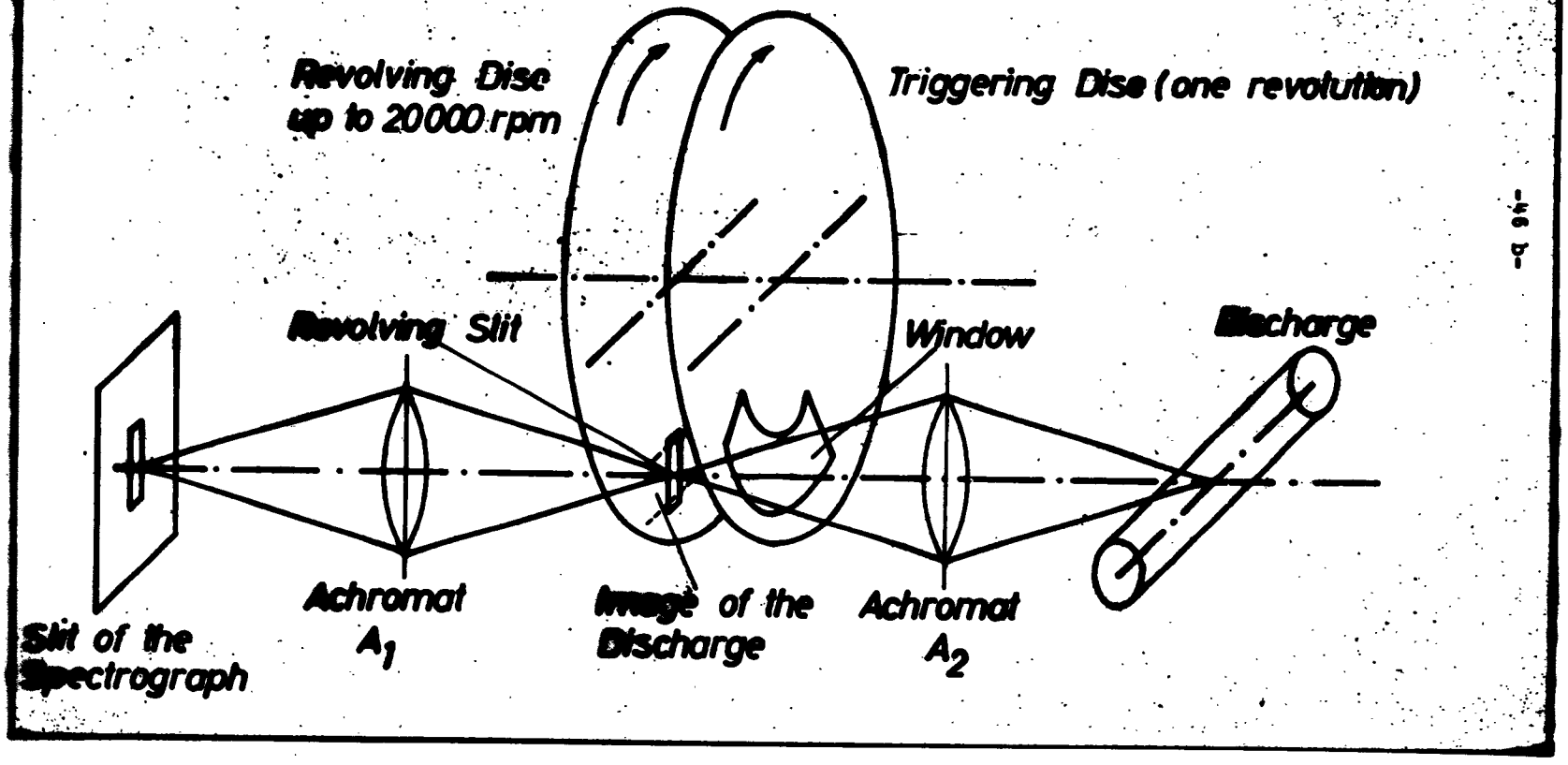

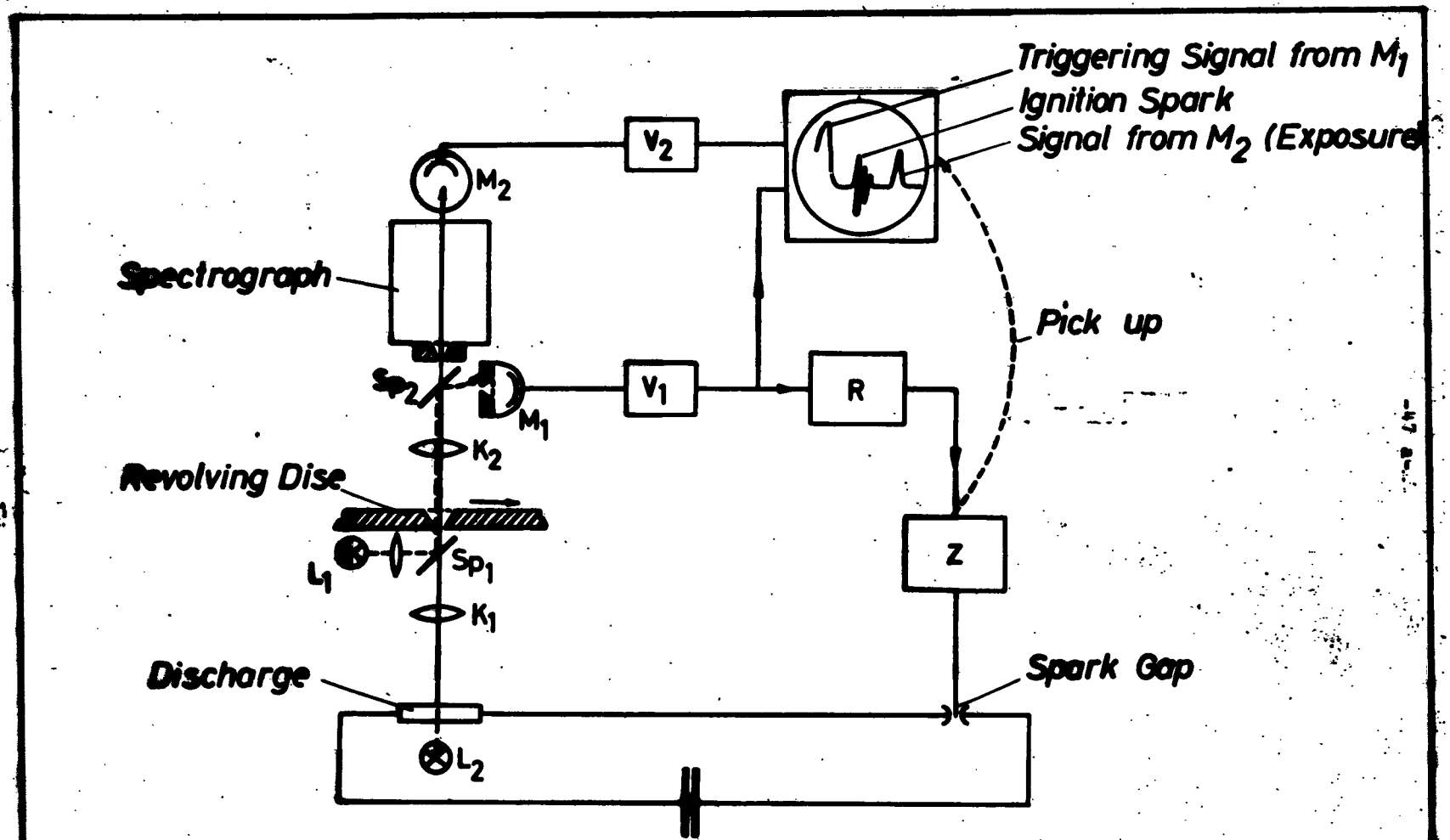

Fig. 23 Synchronization of the Short-time shutter

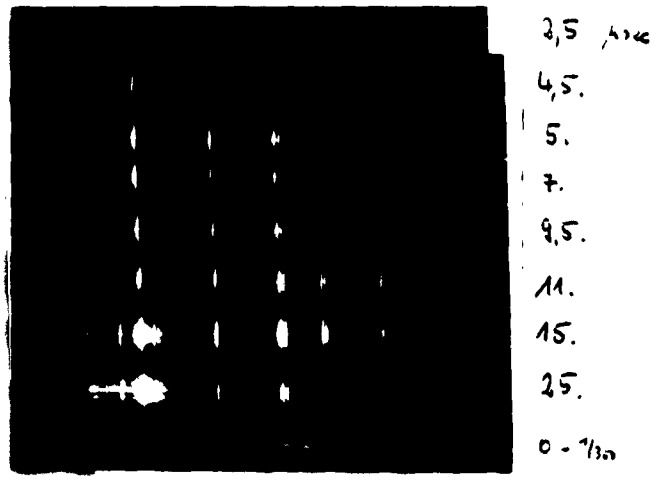

Fig. 24 Spectrum of the Pulsed Discharge at different times

Fig. 25a
Spectrum of the "Fast" Impulse

Fig. 25b
Spectrum of the "Slow" Impulse

Fig. 26 Relative Intensity of a N II, N III, N IV-line

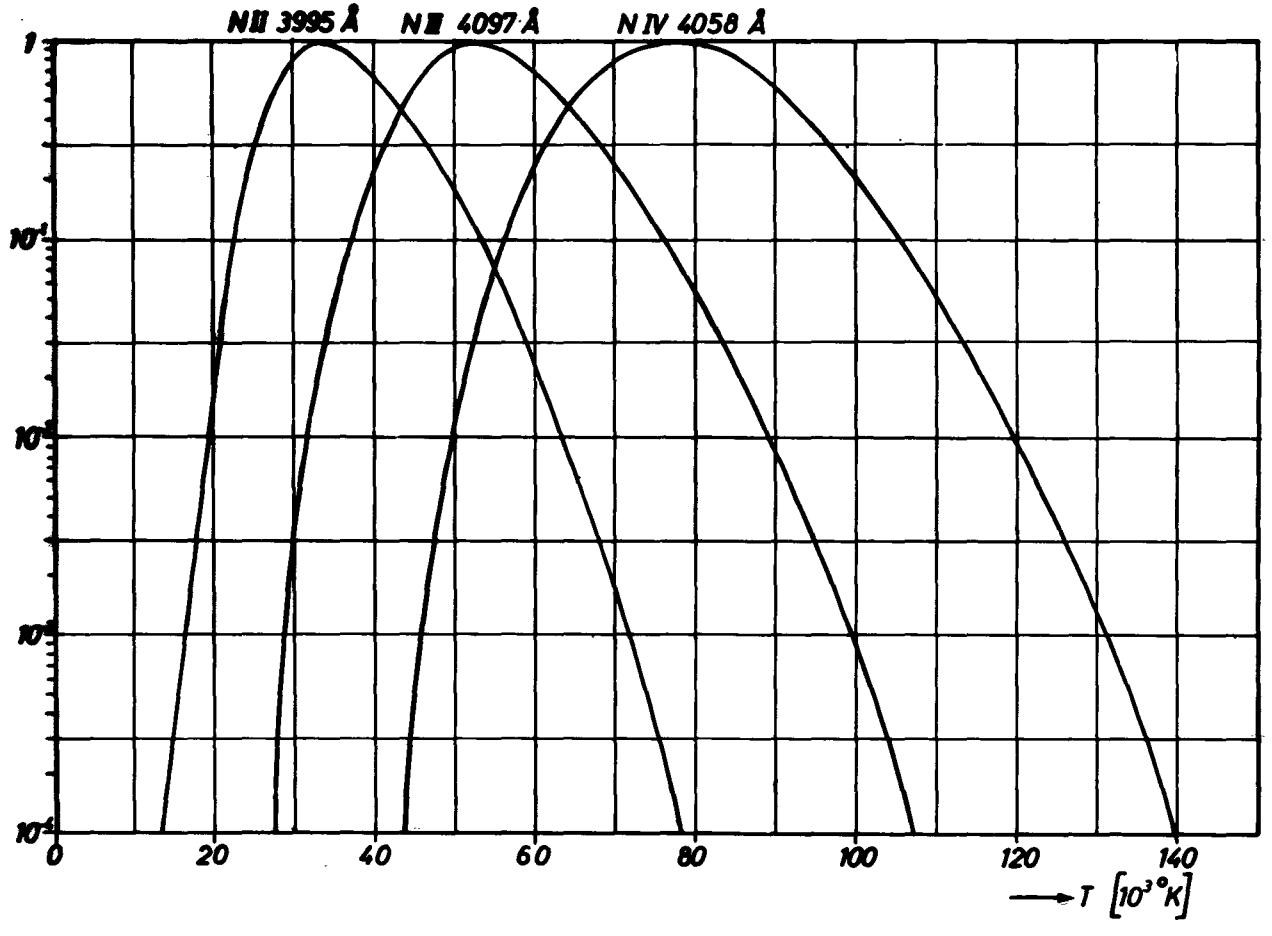

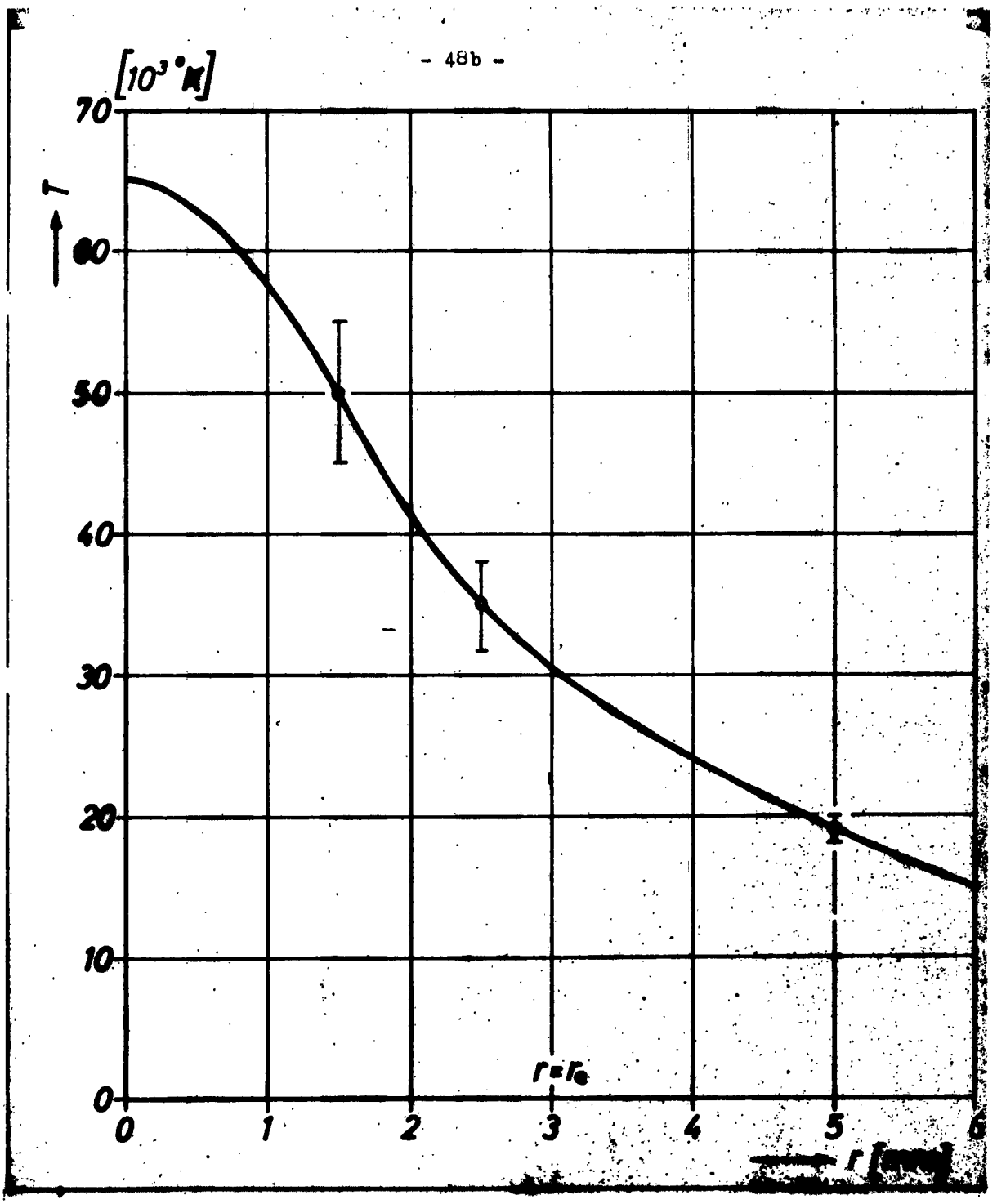

Fig.27 Temperature Profile

3D. Vacuumspectroscopy

In high density plasmas the maximum intensity of the continuous radiation moves to the range of shorter wavelengths. On one hand this is caused by the appearance of higher ionization degrees, on the other hand by the shift of the maximum of the black-body radiation. Under suitable conditions, which in our impulses were partly fulfilled, this goes down to the vacuum Ultra-violet region. Therefore, it seems sensible to investigate the general facilities of the vacuum spectroscopy.

In the case of the hydrogen plasma the line intensities are quite considerable in the vacuum-UV. For instance the Lyman-line radiates black out of a plasma of 1 mm thickness, 17 000 ^{o}K and 1 at. These are about the conditions which are present in a stationary hydrogen arc. Another characteristic of the Lyman-lines which can be used for the measurements, is the following: In the case of our hydrogen plasmas a line broadening which can be measured by means of the vacuum spectrograph, only appears at a pressure of about 10 at (in the visible zone already at 1 at). These characteristics of the vacuum-UV radiation make it possible to investigate plasmas of high density and temperature in this way.

In order to be able to carry out measurements in the vacuum-UV ($400 < \lambda < 1800$ Å) in hydrogen plasmas, several relations between the various plasma characteristics such as continuous radiation, line intensities and temperature must be known.

The following curves were calculated for the requirements of the experimenter:

a) The absorption coefficient $\varkappa$ and the emission coefficient ε of the continuous radiation as functions of the wavelength λ with the reciprocal temperatures Θ = 0,1- 0,5 as parameters ($\Theta = \frac{5040}{T}\left[^{o}K^{-1}\right]$), Fig. 28 and 29. According to Kramer-Unsöld the absorption coefficient per cm is

$$\varkappa_\lambda = \frac{64\pi^4}{3\sqrt{3}} \frac{m_e e^{10}}{c^4 h^6} \lambda^3 \left\{ \sum_{n=1}^{u_4} \frac{e^{u_n}}{n^3} + \frac{e^{u_5}}{2u_1} \right\} n_H e^{-E_i/kT} \qquad (19)$$

where

$$u = \frac{h \cdot c}{\lambda kT} \quad \text{and} \quad u_n = \frac{R\, hc}{n^2 kT} \qquad (20)$$

m_e, h, e, c, k = known natural constants

λ = wavelength

E_i = ionisation energy

T = temperature

g_n = Gaunt-factor

n = 1,2,...

n_H = number of neutral atoms per cm^3

n_H was determined by the Saha formula.

For optically thin layers the emission coefficient is:

$$\varepsilon_\lambda = \varkappa_\lambda \left(1 - e^{-u}\right) B_\lambda(T) \qquad (21)$$

$B_\lambda(T)$ = intensity of the black-body radiation of temperature T and for the wavelength λ

The emission coefficient was calculated this way neglecting the Gaunt-factor ($g_n \approx 1$) and without H^- continuum as its contribution is considerable in the ultra-red.

δ) The line broadening $\Delta\lambda$ for the Lyman-Lines L_α and L_β as functions of the temperature, the pressures being 10 and 100 at. (Examples are given in Fig. 30 and 31). With the aid of the "line profiles" from "Stark broadening of hydrogen lines in a plasma " by H.R. Griem, A.C. Kolb and K.Y. Shen (1960) the broadening of the various Lyman-Lines (L_α and L_β) were calculated as a function of the temperature. It is obvious that an essential broadening of the L_β occrus at about 10 at. In the case of the L_α the broadening does not appear below 100 at.

γ) The relative line intensity of the Lyman-lines L_α, L_β and L_γ as functions of the temperature. The absolute intensity of a spectral line is:

$$J_\nu = A_{n_0 n} \cdot n_n \, h\nu = A_{n_0 n} \frac{g_n}{Z_0(T)} n_0 e^{-E_n/kT} \qquad (22)$$

$A_{n_0 n}$ = transition probability $n \to n_0$
n_n = number of excited atoms in the state n per cm^3
n_0 = number of neutral atoms per cm^3
g_n = statistical weight of upper term
Z_0 = partition function

Since $A_{n_0 n}$ and $h \cdot \nu$ do not depend on the temperature, one obtains:

$$J_\nu = \text{const} \cdot n_n \sim e^{-E_n/kT} \cdot n_0 \qquad (23)$$

n_0 was calculated from the Saha formula (Fig. 32).

For the experimental investigation of plasmas in the UV region (3 300 - 400 Å) we use a Hilger vacuum-grating-spectrograph. The instrument operates according to the Rowland principle.

Data:	Reflection grating	8 x 5 cm
	(at the same time imaging system)	5 700 lines/cm
	diameter of Rowland circle	3 m
	Dispersion in the first order	5,9 Å/mm

For the evacuation of camera and spectrograph two rotary pumps and two oil diffusion pumps are used.
Pump capacity of the rotary pumps: 6 resp. 28 m^3/h
Pump capacity of the oil diffusion pumps: 250 resp. 500 l/h
The scheme of the vacuum apparatus is represented in fig. 33.
For the calibration we applied two methods:

a) A comfortable calibration method up to 1 850 Å is the calibration with the aid of an iron spark spectrum. The light comes into the spectrograph through a LiF-window. The iron spark burns in air and is generated by means of a Fuess spark generator. The spectral lines of the iron spectrum are identified with the aid of a wavelength table and layed down in an iron atlas (see fig. 34). The iron atlas consists of 9 pages.

b) If a calibration over the entire wavelength range of the spectrograph is desired, one has to work without window, since the usual window materials absorb the radiation from a certain wavelength on, which is still within the

wavelength range of the spectrograph. For this purpose a low pressure discharge vessel was developed which is operated by means of high voltage impulses of 4 kV (see fig. 35 and 36).

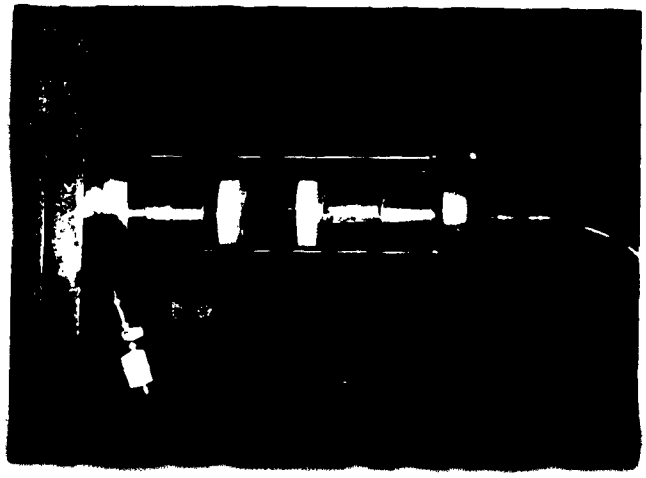

Fig. 36
Argon Discharge Chamber

The discharge takes place in Argon gas in a narrow channel and is being contracted at the same time in order to obtain a higher light density. The gas flow in the discharge vessel is constant. By means of a pump the Argon is extracted from the zone between the discharge vessel and the spectrograph slit, in order to retain the vacuum in the spectrograph. -

Thus the Argon arc spectrum was obtained which serves as a basis of an Argon line atlas (3 500 - 500 Å), see fig. 37.

Investigations in the Vacuum-UV above 1 100 Å can be carried out by means of a LiF-window. Below this wavelength there is no material which is penetrable for the radiation. Therefore,

an apparatus was developed (see fig. 38 - 42) which allows the spectroscopic investigation of the high pressure arc without window. The pressure of 1 at is reduced in 4 steps to the vacuum of the spectrograph. The first two steps of the vacuum sluice are evacuated by means of mechanic pumps, the last two steps by means of oil diffusion pumps. Between the fourth step of the vacuum sluice and the spectrograph there is a valve, which allows a separation of the pressure in the spectrograph and the vacuum sluice.

The valve has a LiF-window which can be penetrated by the light down to 1.100 Å. Just in front of the vacuum sluice there is a vacuum-tight shutter which at the same time serves as an optical shutter. This shutter allows different opening times, the shortest in our case being 1 ms. By this it is possible to use larger diaphragms without affecting the vacuum in the spectrograph. These short opening times are mainly intended for impulse plasmas, for the triggering of which the shutter is equipped with an optical setup. The arc which is to be investigated side-on burns immediately in front of the shutter. It is surrounded by an Argon coat, since the UV radiation passes it without noticeable absorption losses. The distance arc-spectrograph slit is 23 cm. This arrangement allows the approximation of a stigmatic image due to large depth of focus of the spectrograph. The imaging by means of mirrors was not carried out because of the high reflection losses.

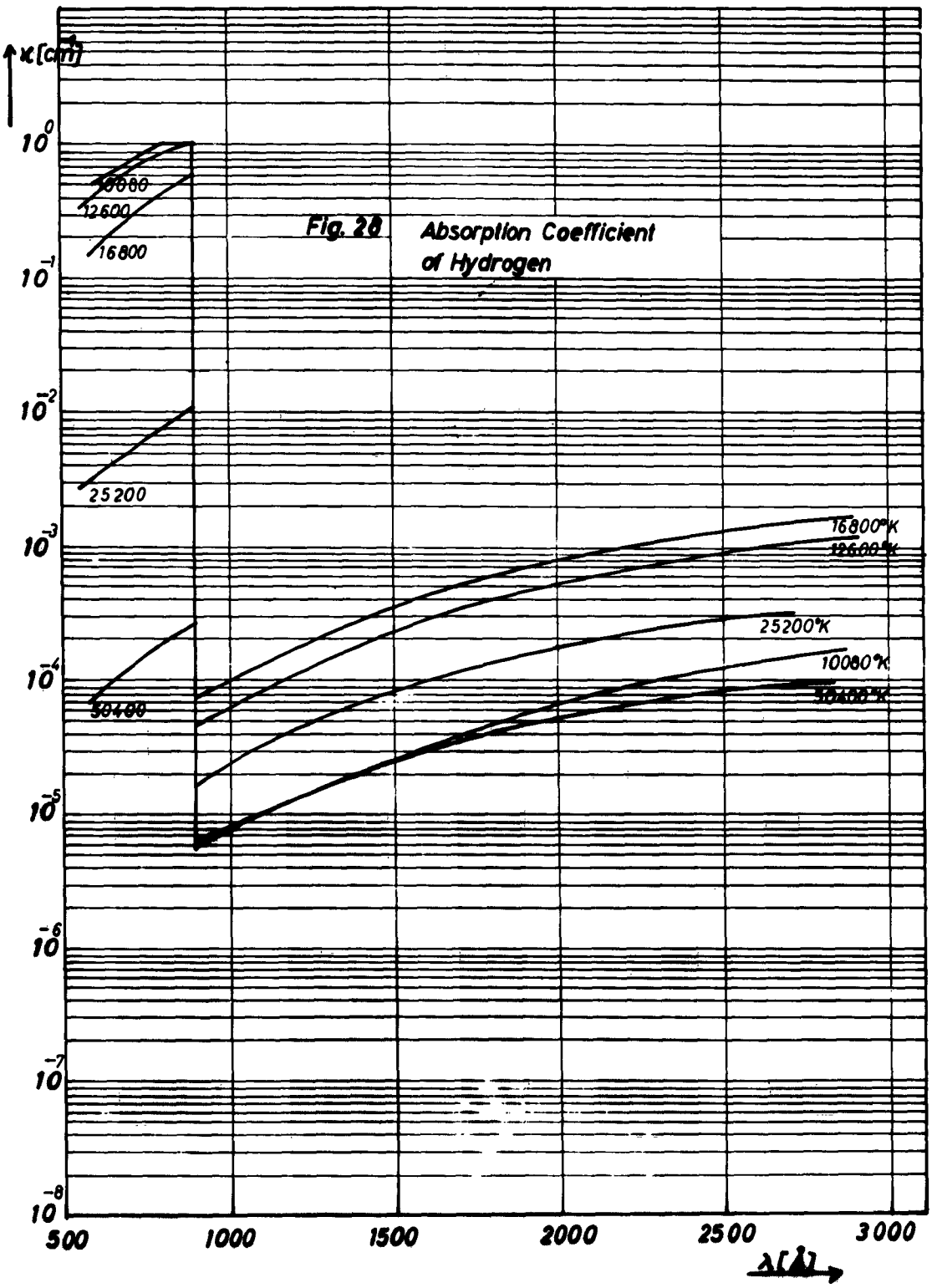

Fig. 20 Absorption Coefficient of Hydrogen

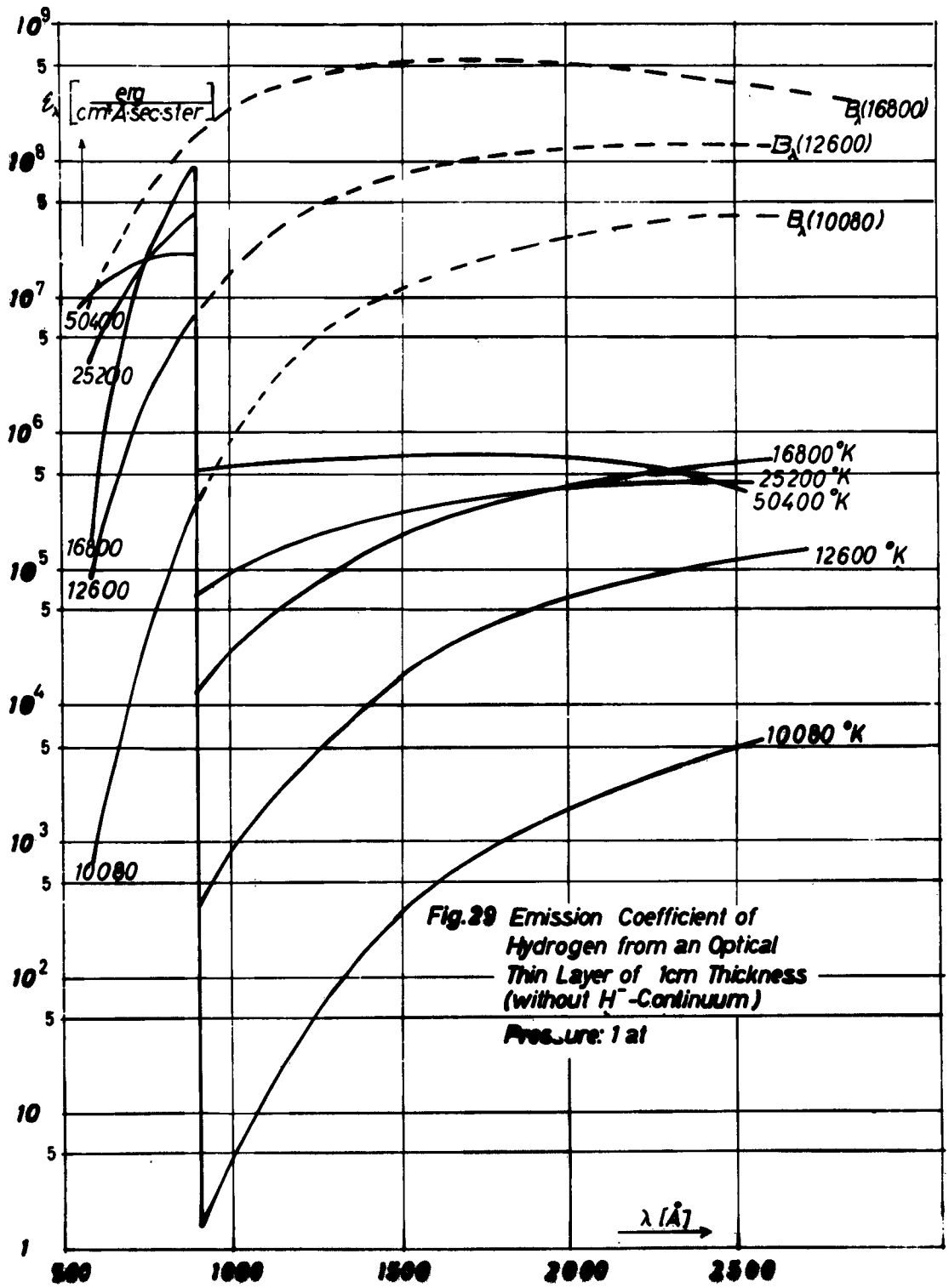

Fig. 29 Emission Coefficient of Hydrogen from an Optical Thin Layer of 1cm Thickness (without H^--Continuum)

Pressure: 1 at

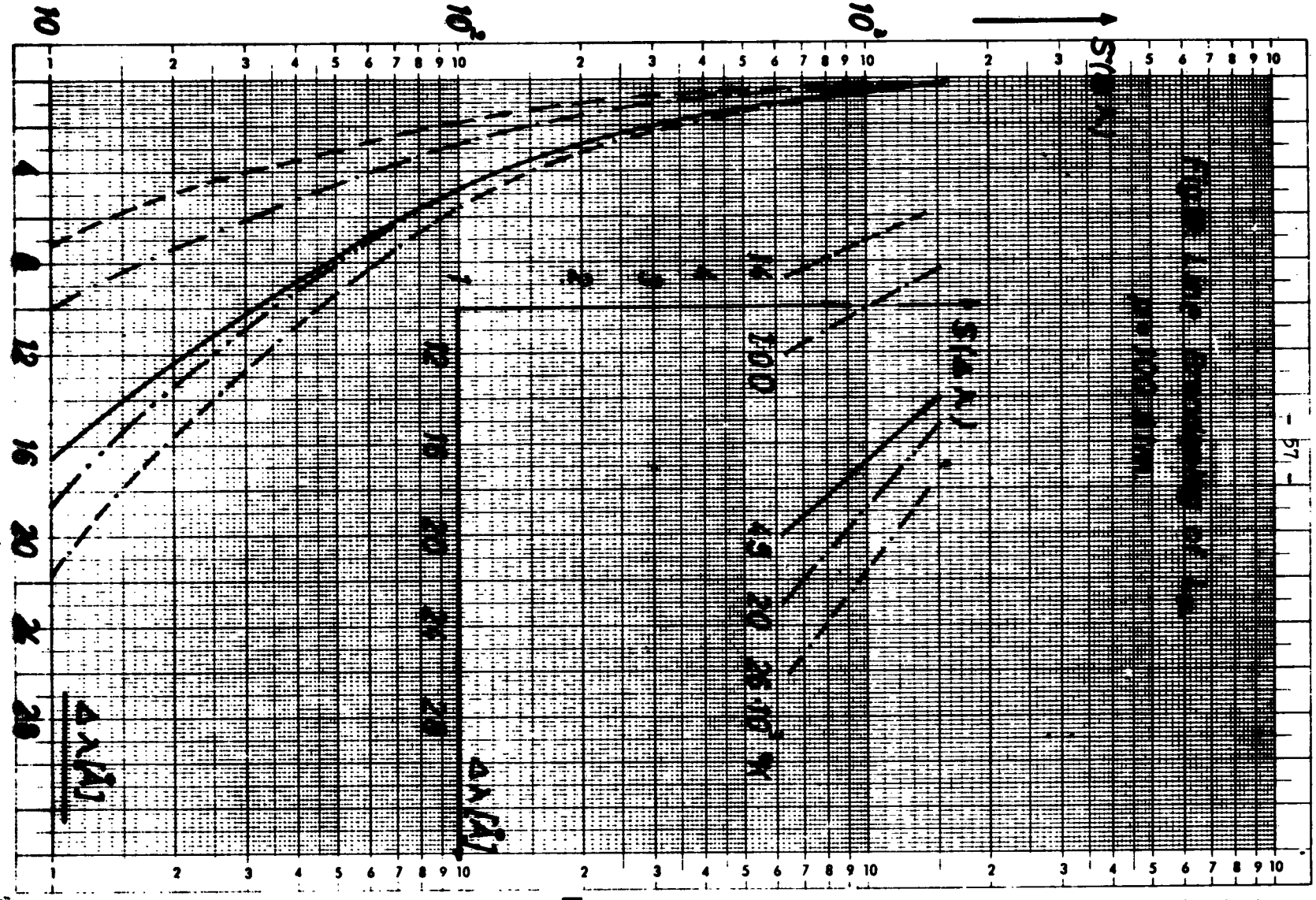

Nr. 373·½ A 4 P

Eine …nse logar. geteilt von 1 bis 1000, Einheit 90 mm, die andere in mm

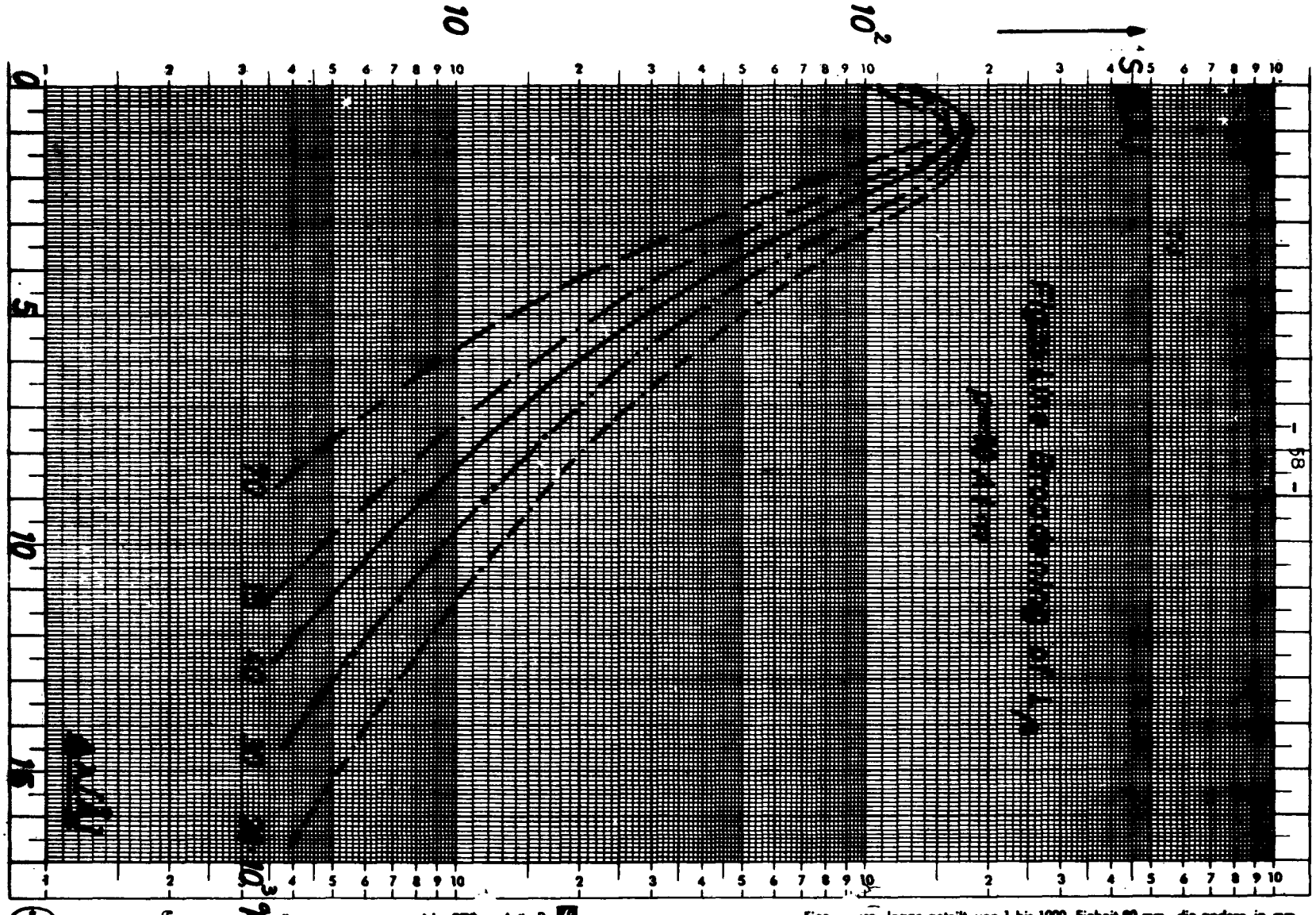

Fig. Line Broadening of L_β
p=[illegible] Atm
S
10^2
10
10
15
20
30
40·10^3
0
5
10
15
$\Delta\lambda$ Å

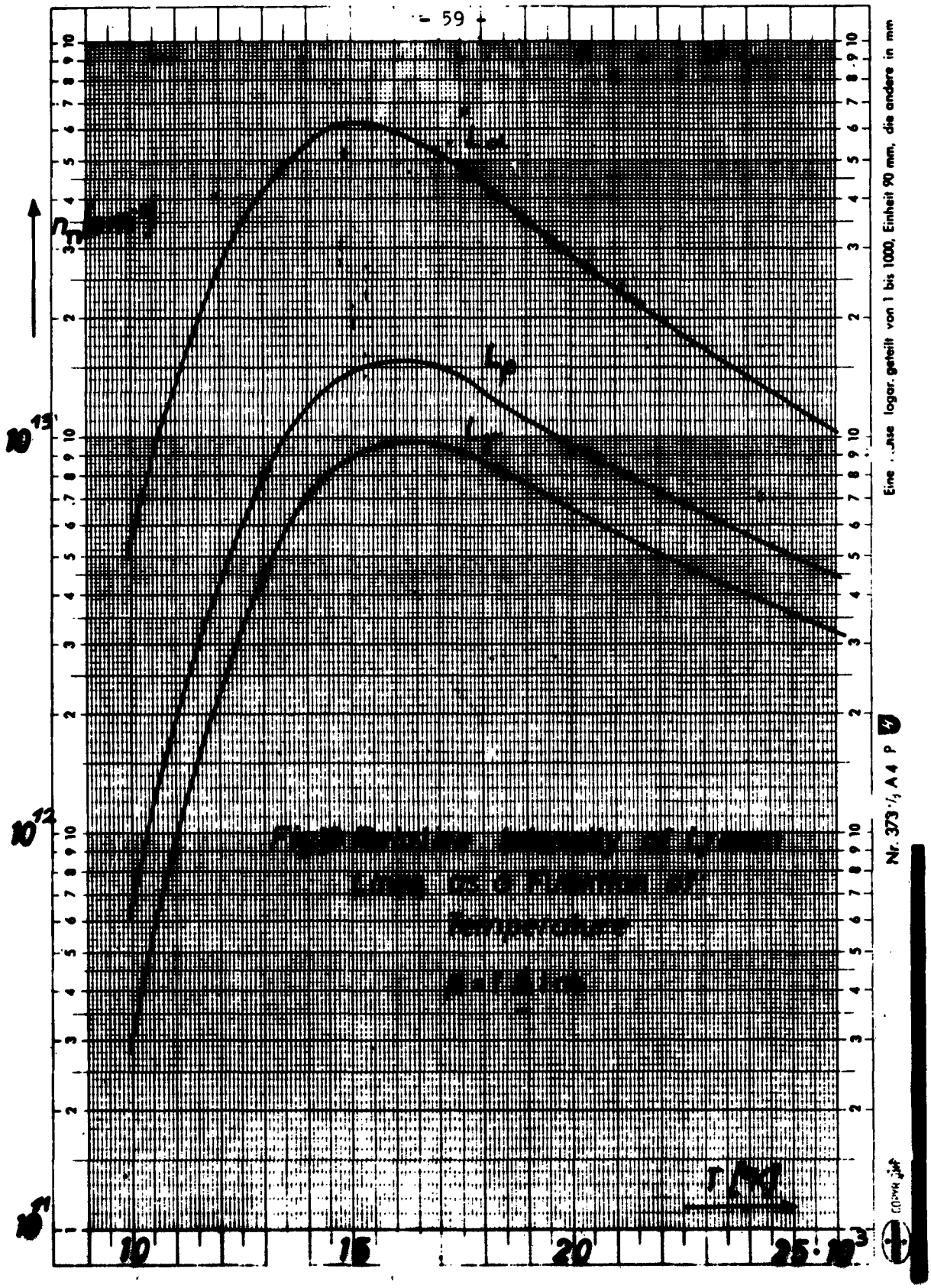
Eine ...ase logar. geteilt von 1 bis 1000, Einheit 90 mm, die andere in mm
Nr. 373 ½ A4 P

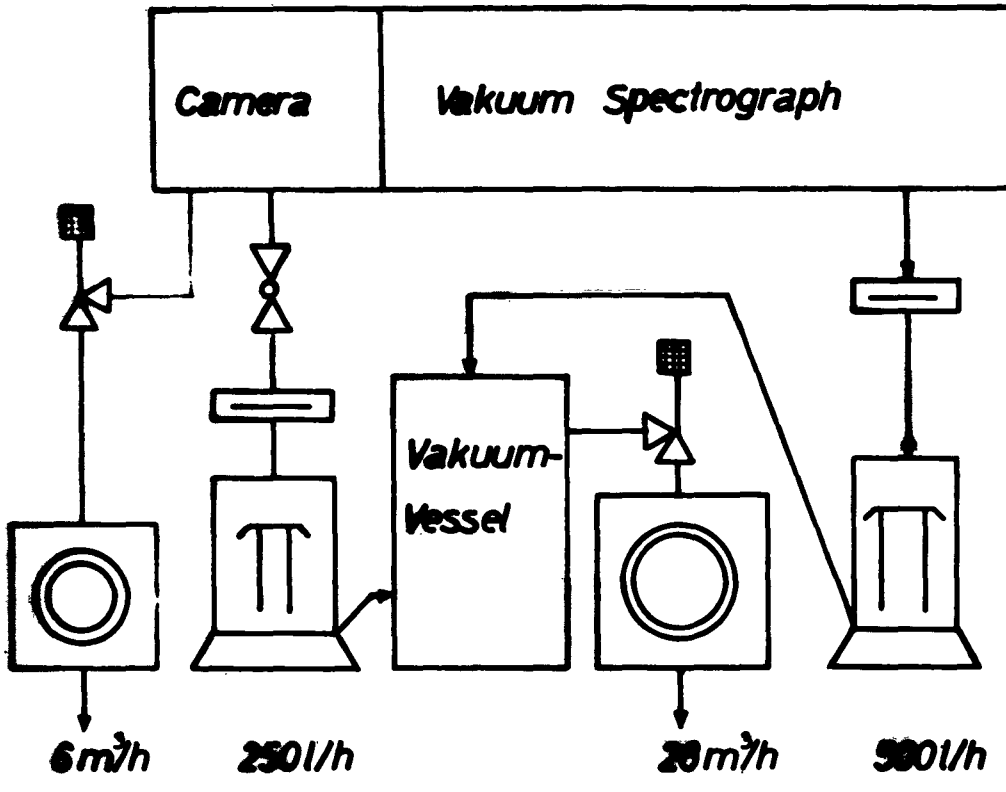

Vakuum Supply for the Vakuum Spectrograph

Fig. 33

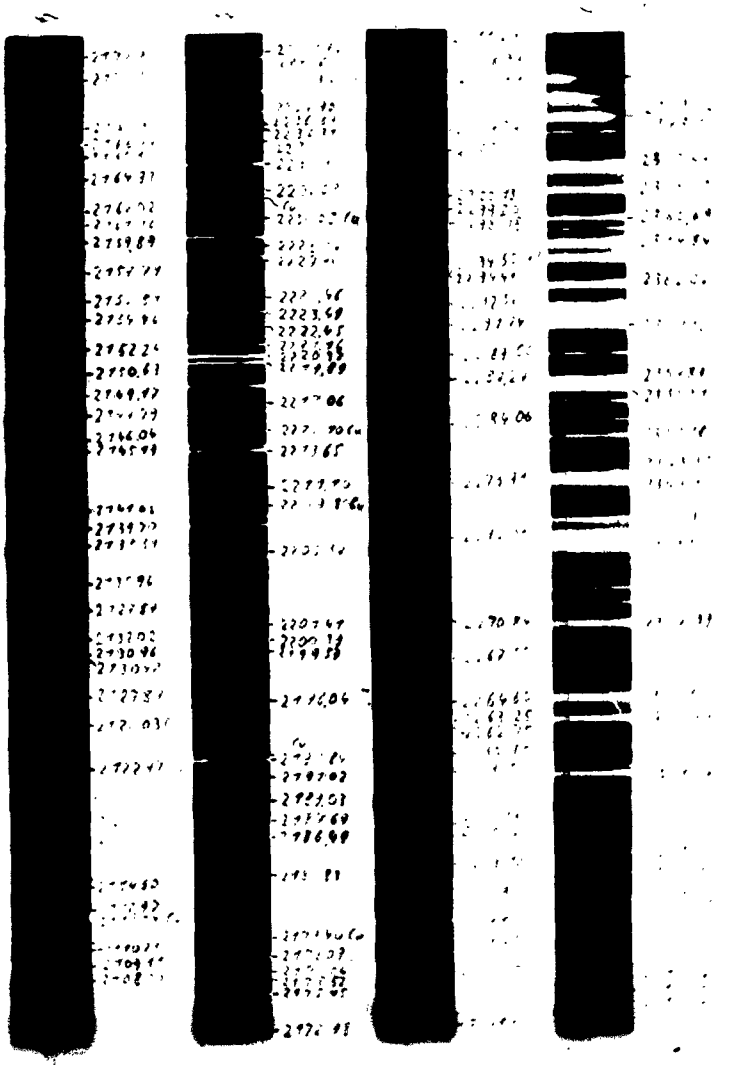

Fig. 34 Iron Atlas

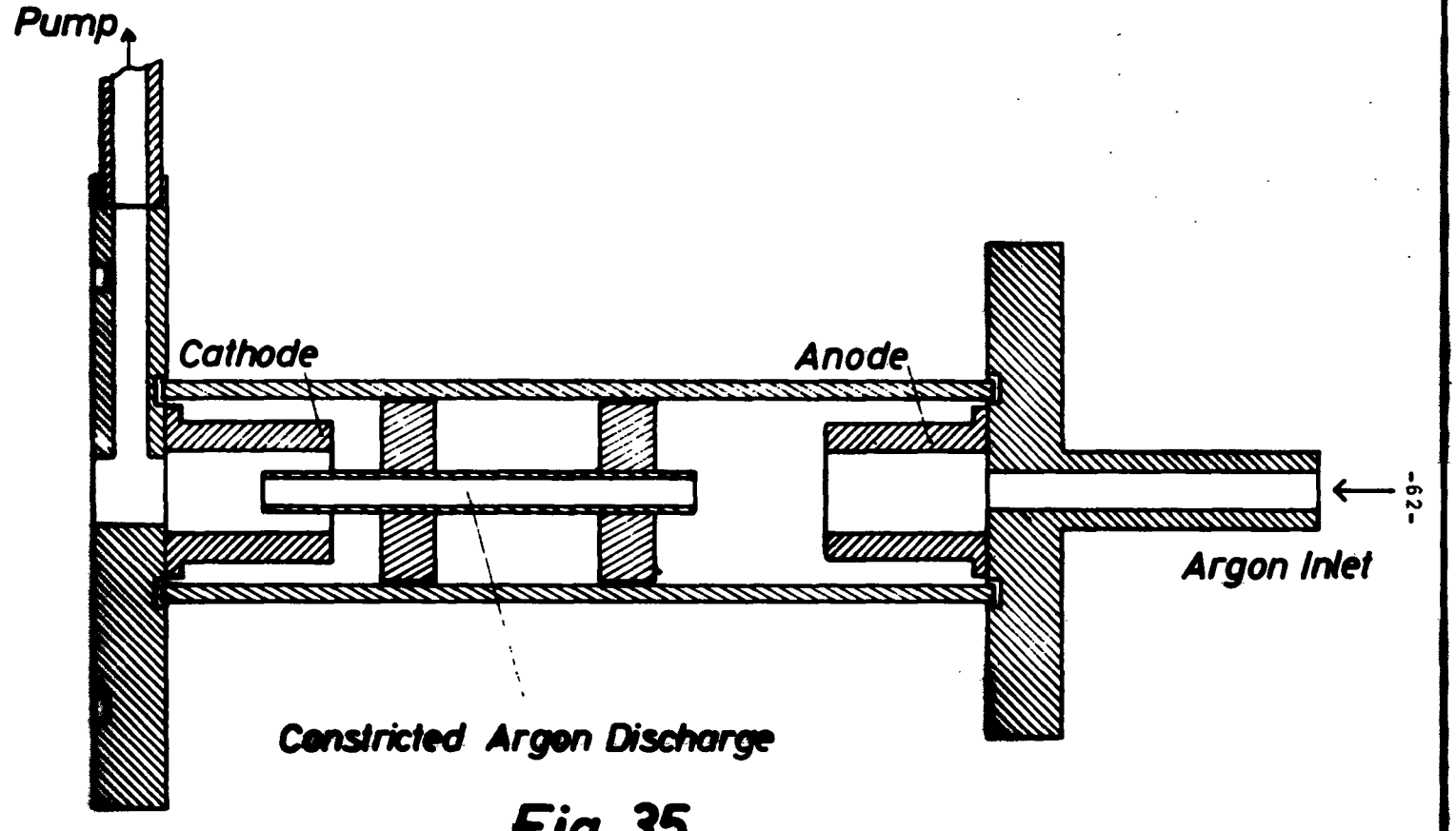

Fig. 35
Light Source for Calibration with the Argon Spectrum

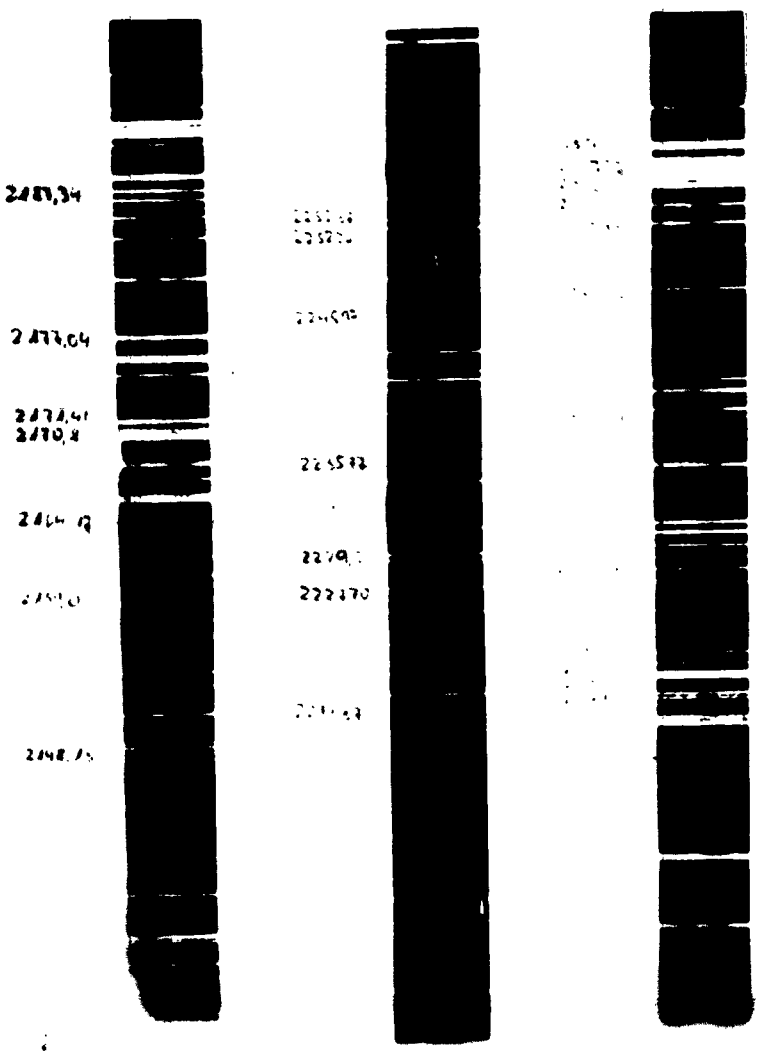

Fig. 37 Argon Atlas

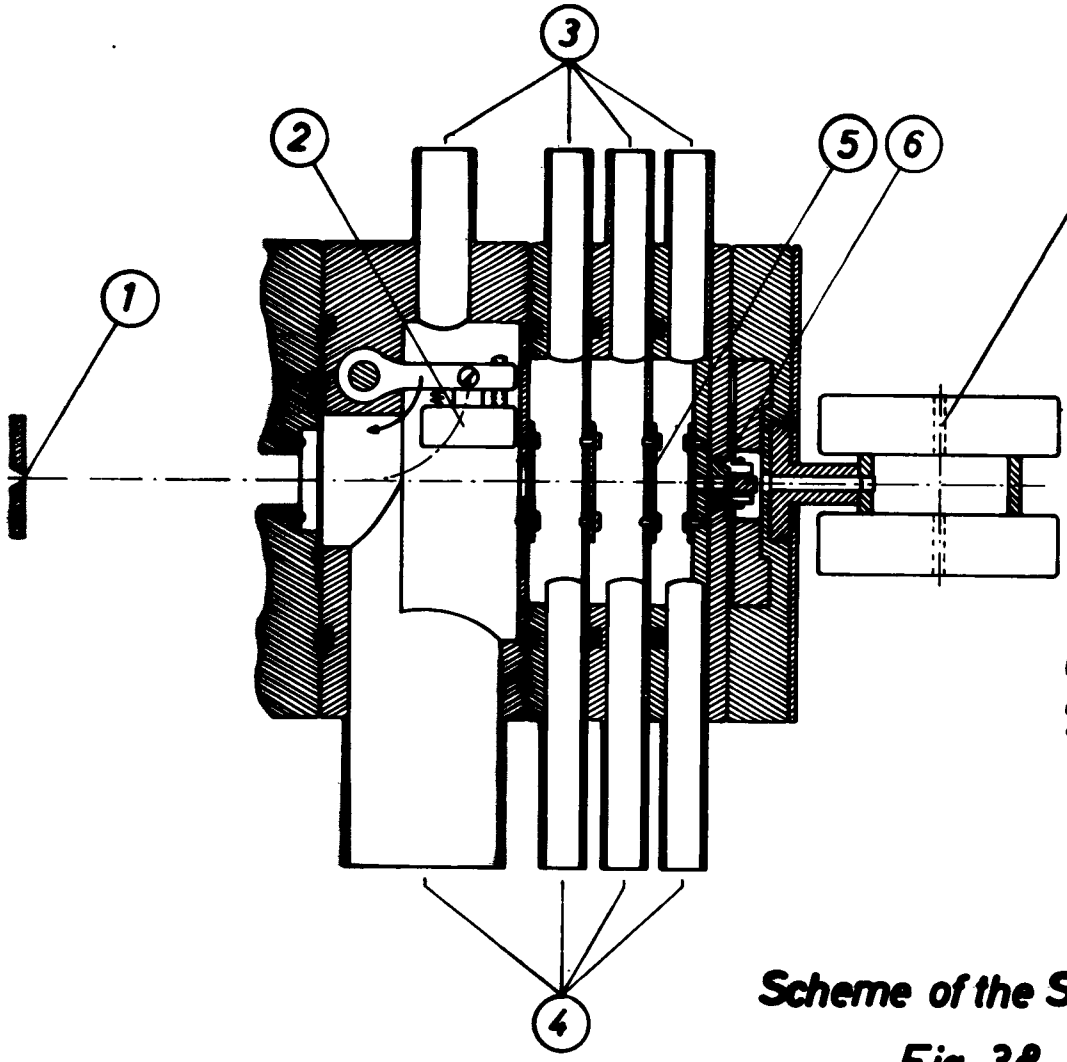

1 Slit of the Spectrograph
2 Valve Cover
3 Manometer Connections
4 Pump Connections
5 Exchangeable Diaphragm
6 Slide of the Shutter
7 Arc Chamber

Scheme of the Sluice

Fig. 38

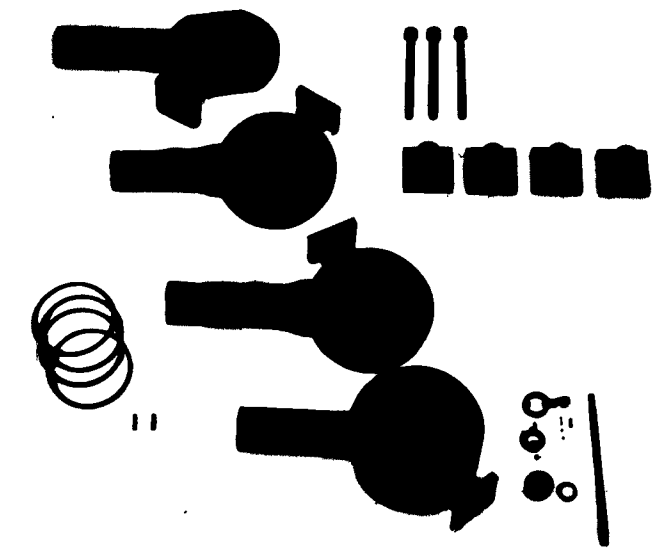

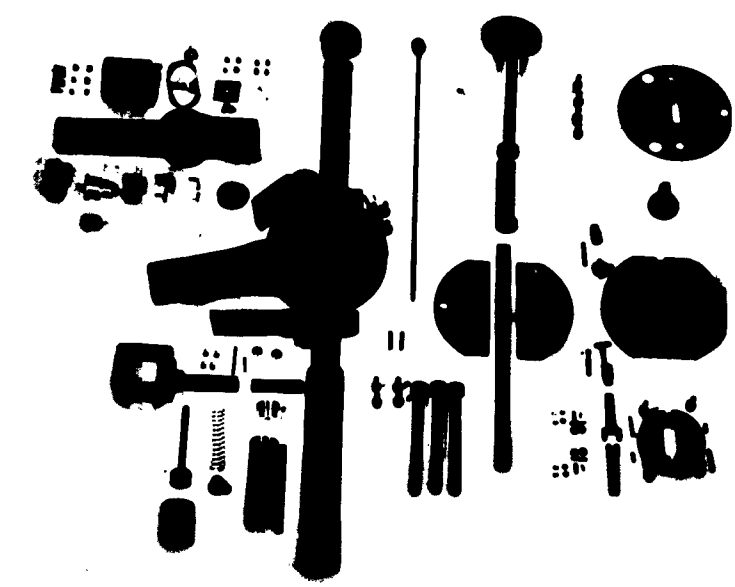

Fig. 39, 40 Vacuum Sluice

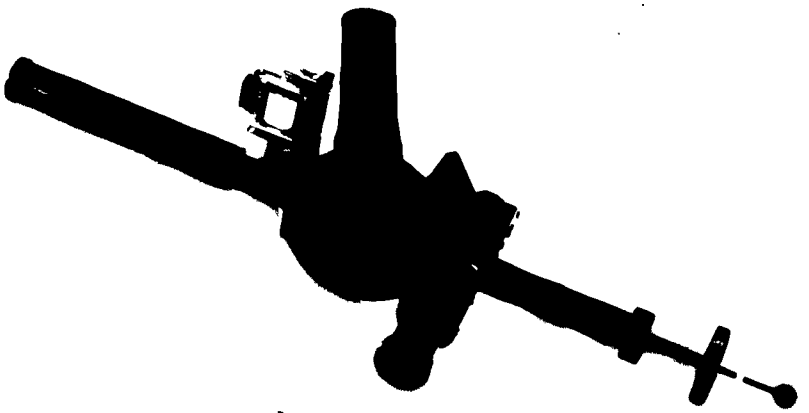

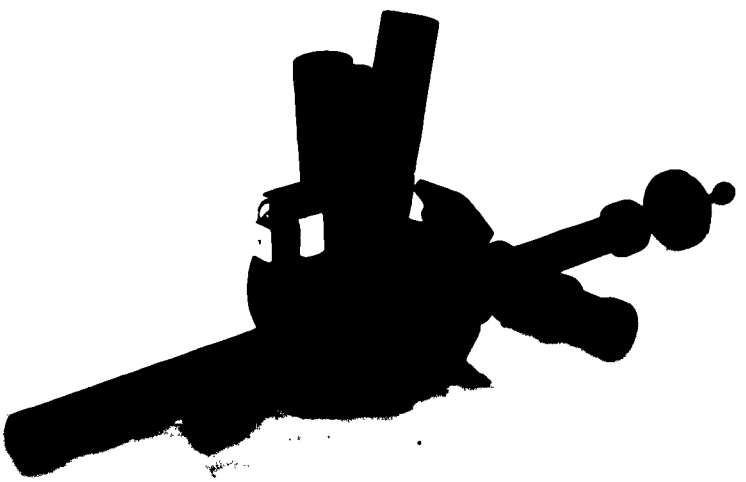

Fig. 41,42 Vacuum Sluice

3E. Evaluation and Discussion of Experimental Results.

The theoretical problem is the determination of the behaviour of the plasma channel with a given time variation of the current.

In order to simplify the mathematical problem, the experiment is based on a channel model (Schrade, 1961). This model has 3 coaxial zones with different radii. The central zone is the proper plasma zone which is supplied with the electric energy. This zone is expanding and by this effecting a change of the parameters in a second zone, the outer limitation of which is characterized by sound velocity x time, respectively shock wave velocity x time. The third zone is the undisturbed cold gas coat. If the mathematical equations (1-3) are applied to this model, we obtain instead of the simultaneous partial differential equations a system of ordinary differential equations. This allows the description of the time-dependent behaviour of temperatures and particle densities of the individual components, as well as the channel radius (= radius of the central zone). Here the influence of the outer zones is taken into consideration. The stability behaviour of the discharge channel was continuously controlled.

The calculations were carried out on an electronic computer of the type ER 56 (Standard Electric Lorenz).

The theoretical results are given in figures 44 a-b. The lowest curve in each figure shows the current variation on which the calculation in the central zone is based. It

corresponds to the current variation found by means of magnetic probe measurements (see fig. 43). The current maximum is about 6 kA. We tried to employ a curve for the current variation with faster increase and higher maximum current. The initial conditions given by the pre-discharge were retained. However, this new curve yielded discrepancies which only vanished again after a reduction of maximum current and rate of increase.

These mentioned discrepancies are the following: If maximum current is increased beyond a critical value (larger than approximately 10 kA), the calculations yield a contraction of the plasma channel due to the magnetic forces. At the same time the ohmic part of the electric field strength increases rapidly. Such a behaviour is not deemed possible from theoretical considerations for our arrangement and was also never observed experimentally in our device. From this we conclude that the maximum current of the plasma channel must not become larger than 6-9 kA. As in our experiments total current intensities of 50 to 150 kA were measured, it can be assumed that the major portion of the current had to flow over surrounding zones.

We pretend that this is caused by the generation of particle carriers outside the central zone by means of photons and wish to demonstrate it by the following calculation. The number z of the photoionisation of particles in the quantum state n is according to Elwert (1952)

$$\varepsilon = n_{o,n} \cdot \frac{16}{\sqrt{3}} \frac{\Phi}{\alpha^3 c^2} \frac{\zeta_n n \nu_n^3}{Z_{eff}^2} Ei\left(\frac{\chi_n}{kT_s}\right) \cdot V \cdot f , \qquad (24)$$

$n_{o,n}$ = Density of atoms in the quantum state n

Φ = $\frac{8\pi}{3} \frac{e^2}{m_e c^2} = 6{,}6 \cdot 10^{-25}$ cm^2

n = Main quantum number

Z_{eff} = $\left(\frac{\chi_n}{\chi_2}\right) n^2$

α = $\frac{e}{c\hbar}$ Fine-structure constant

ζ = number of electrons in the same shell

ν_n = limiting frequency

f = uncertainty factor between 0,6 and 1

V = dilution factor

χ_n = ionization energy

This formula was derived by means of the Planck radiation intensity in the Wien approximation $\exp.\frac{h\nu}{kT_s} \gg 1$. Since the discharge channel is a black-body, the formula is applicable. Instead of the radiation temperature T_s we put the electron temperature. If we limit ourselves to the zones immediately surrounding the plasma zone, the dilution factor V has the dimension 1.

Assuming that the radiation temperature is about 50 000 ^{o}K, as this is certainly the case in the discharge channel, we obtain the number of the photoionizations which amounts to 10^{24} per cm^3 and s, provided that the atomic density is 10^{18} particles per cm^3 (ionization energy of nitrogen atoms = 14,5 eV, basic state n = 2). In a time of 10^{-6} s which corresponds

to the discharge time up to the maximum current density, about 10^{18} particles are ionized by means of radiation. The particle carriers are accelerated in the electrical field and heat the outer gas.

The upper parts of fig. 44 a-b show the ionization degree, the electron and ion temperature, the ohmic field strength and the time-dependent variation of the radius in the central zone. It can be seen that towards current maximum the latter increases by about 50 %. The electron and the ion temperatures only differ from each other in the first phase of the discharge. At the beginning of the discharge the "ion temperature" is about the same as the temperature of the neutral gas particles. Both temperature curves approximate each other quickly, as soon as the heavy particles become charge carriers and the cross section of the Coulomb forces gets effective.

From about 0,8 µs the temperature remains nearly constant. However, it is interesting to note that the reaction has not yet stopped. Only after about $5\text{-}6 \cdot 10^{-7}$ s the curves for N^{++} and N^{+++} are horizontal, i.e. the reaction equilibrium is reached. From this we can conclude that the relaxation time of the ionization reactions is approximately 10^{-6} s which corresponds to the estimation.

Furthermore, it is remarkable that only a small percentage of the Joulean heat expended in the plasma channel is used for the heating. Table 2 shows how the Joulean heat which is put into the electron gas, is distributed over the various loss mechanisms.

Table 2: Energy balance of electron gas for two different times after the start of the heating.

Time	10^{-7} s	10^{-6} s
Input (Joule) energy	100 %	100 %
Energy losses caused by:		
Radiation	23 %	94 %
Reactions	66 %	5,4 %
Heat exchange	10 %	0,1 %
Volume work	0,2 %	0,3 %
Heat conduction	0,1 %	0,2 %
For further heating remains	1 %	0 %

After 10^{-7} s, i.e. the highest temperature increase, the reaction losses are dominating, followed by the radiation losses (23 %) and the energy losses by heat exchange (10 %). After 10^{-6} s the temperature increase stops. The radiation consumes most of the energy, for the reactions remain only 5,4 %. As can be seen from our spectroscopic measurements, the discharge channel is nearly a black-body. This is true for all elements with higher atomic number.

The pressure in the central zone amounts to about 10 at. This is due to:

1. the magnetic compression
2. the inertia of the outer gas which was considered in our model as boundary condition.

The result of our calculation is a maximum temperature of 65 000 ^{o}K. This temperature does not depend much on the changes in the given curve I (t), provided that there are no

discrepancies in the calculation itself. Our probe measurements indicate axis temperatures between 80 000 and 90 000 °K; The spectroscopic measurements described above give the same axis temperatures of 65 000 °K, which we have calculated. However, as the Saha equation is applied and a reaction equilibrium does not exist, these temperatures seem to be too low, especially near the axis, so that the coincidence with the theoretical calculation is only casual. 70 - 80 000 °K are estimated to be the most probable values.

4. The Hydrogen Heating.

The theoretical investigation of the discharge process in hydrogen is dealt with comprehensively in a separate paper, which will be submitted shortly as a technical note by H. Schrade (1963). The following gives some general information on the calculations made.

The starting point of the heating is a nearly fully ionized arc channel, while in the case of nitrogen the ionization degree was only 10 %. During the heating process we must not take care of radiation or any reactions between the various ionization degrees. The limitation of the heating process is not due to loss mechanisms but to the instabilities of the discharge channel which are caused by the strong proper magnetic field and the lower inertia of the outer gas. This brings about considerable difficulties which are not found in case of the nitrogen experiment.

Our calculations were performed for current rises to 10^4 A in 1 /us and 10^5 A in 1,5 /us. In the first case the theoretical electron and ion temperatures amounted to 170 000 ^oK. In the second case there appear heavy instabilities at less than 10^{-7} s after starting the discharge. At this moment the temperature in the discharge channel amounts to $3 \cdot 10^5$ ^oK. Since the instabilities imply an expansion of the discharge cross section, a noticeable temperature increase beyond this value should not be possible.

As compared to the nitrogen impulse the hydrogen impulse shows a low radiation loss. Here the electron heat conducti-

vity is decisive. At high current intensities it is possible to reduce the heat conductivity by means of the proper magnetic field of the arc. However, this fact can not be observed, as the mentioned instabilities do not allow the necessary heating.

The theoretically predicted instabilities are proved experimentally. The instable behaviour complicates the measurements. Up to date they have made it impossible to give an adequate quantitative description of the hydrogen impulse. Nevertheless, certain stages of this instability are rather attractive, though they are not reproducible. At the moment we try to confirm this behaviour with the aid of image converters, smear and framing cameras. Fig. 45 a,b,c,d,c show five different stages of the hydrogen impulse discharge at 0,1, 0,3, 0,5, 1,3 and 1,6 µs after the beginning of the discharge as registered by an image converter. The opening time of the image converter was about 50 ns. The stationary predischarge was not registered owing to the low radiation intensity of the arc.

The first stage of the impulse discharge (at 0,1 µs), which corresponds to a current of 13 kA, only causes a slight blackening of the film. It can be seen that the channel is already rather deformed which corresponds to theory. The increase rate of the instabilities grows rapidly after 0,06 µs if we assume a current rise of approximately 10^{11} A/s.

During the heating process the plasma contracts more and more and apparently becomes a plasma ball. If the luminous

zones are the current carrying zones, this contraction may perhaps be explained by the magnetic forces of the originally screw-shaped plasma.

In order to investigate this behaviour, other diagnostic methods were applied, for instance smear camera photography. These show the expansion of the discharge and cloud-shaped intensity fluctuations, which correspond to the screw lines in fig. 45 a-c. A plasma ball could not be isolated on these photographs. However, the experimental material is not yet sufficient in order to allow final statements.

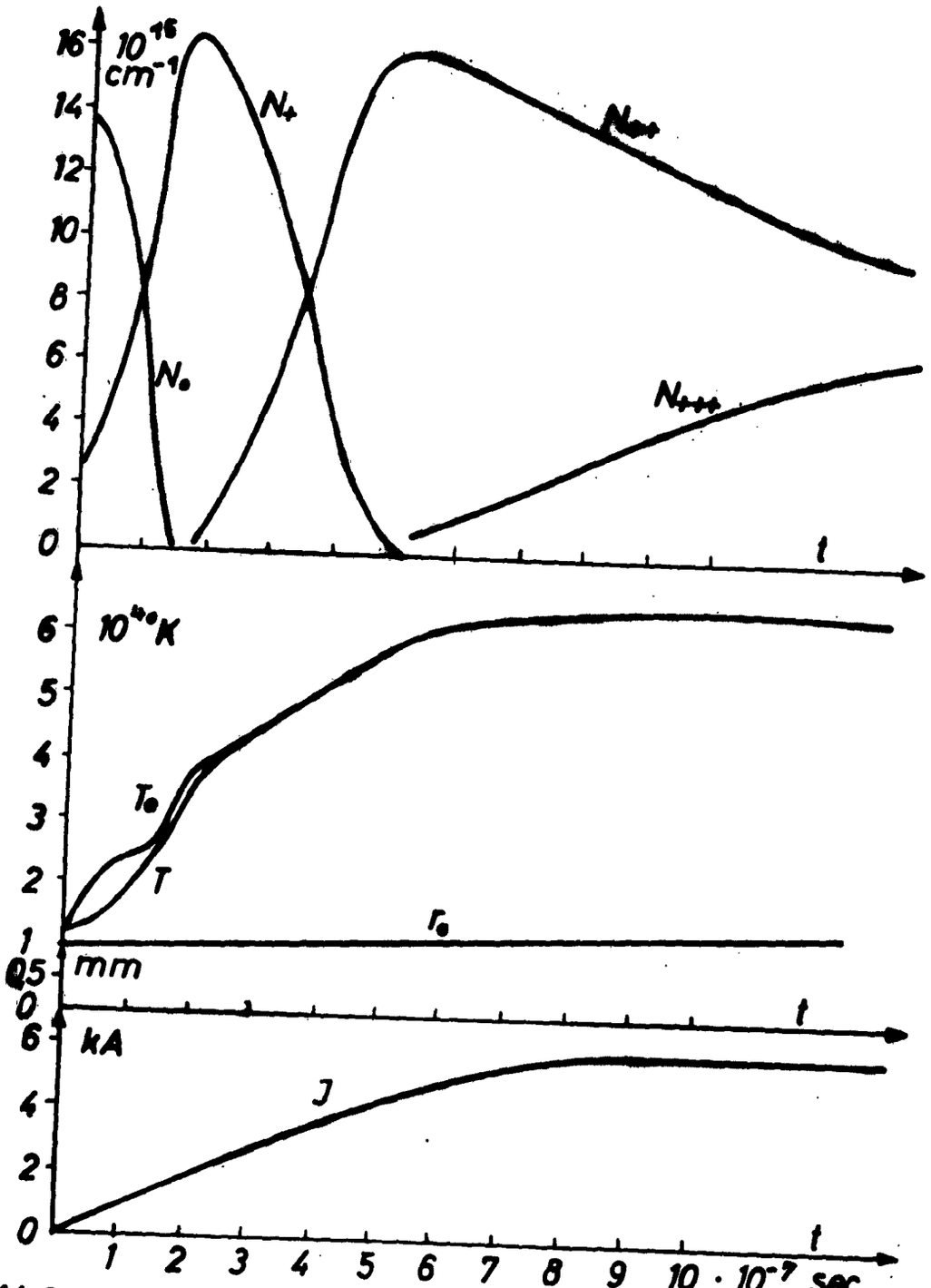

Fig. 44. Composition of Particles of Electron- and Ion Temperature (T_e, T) and of the Radius of the Discharge Channel with Given Current J(t).

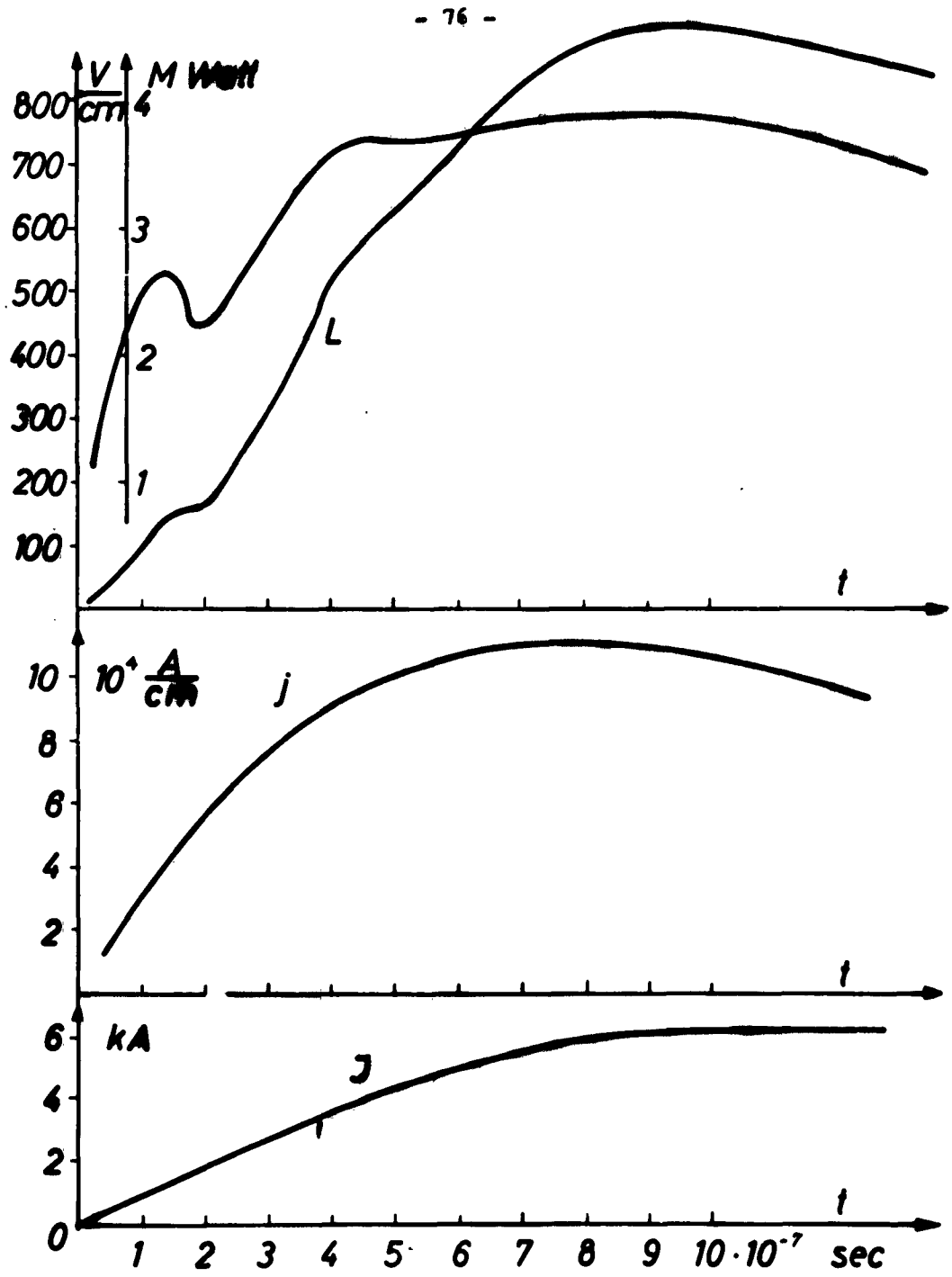

Fig. 44 Current Density j and Electrical Power $h = J \cdot E_{arc}$ as a Function of Time with Given Current J(t)

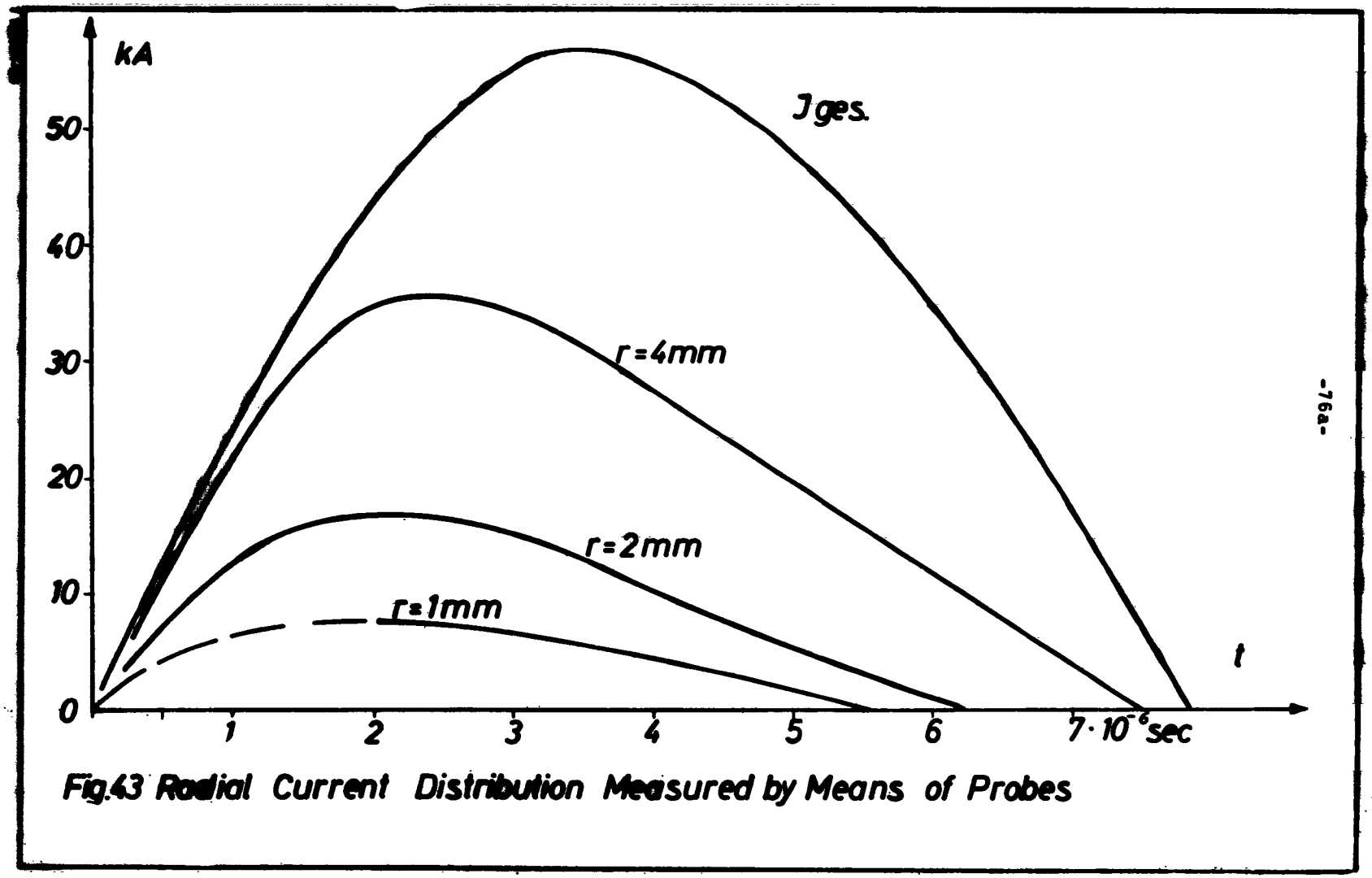

Fig.43 Radial Current Distribution Measured by Means of Probes

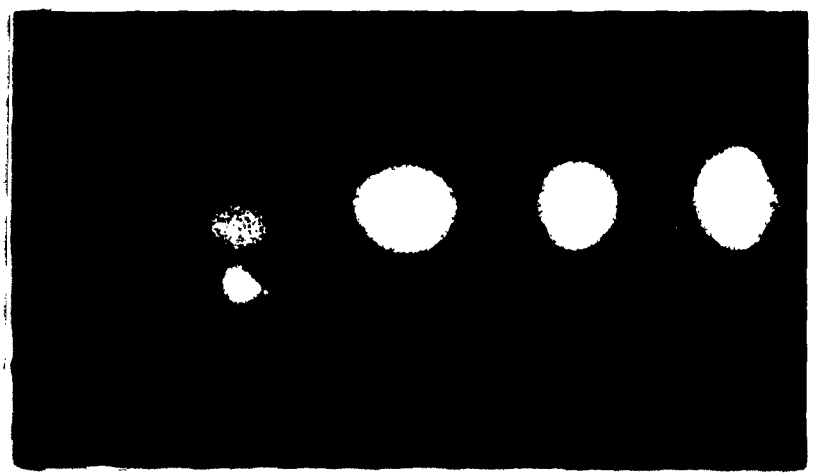

Fig. 45 Photographs taken with an Image Converter 0,1; 0,3; 0,5; 1,3; 1,6 µs after the ignition of the Impulse.

References

ELWERT, G., 1952: Z. Naturforsch. 7a, 432

FINKELNBURG, W. and H. MÄCKER, 1956: Handb.d.Phys. XXII,254

GRAD, H., 1949: Comm. Pure Appl. Math. 2, 331

GRIEM, H.R., A.C. KOLB and K.Y. SHEN, 1960: Phys. Rev. 116, 4

HIRSCHFELDER, I.O., C.F. CURTISS, and R.B. BIRD, 1954: Molecular Theory of Gases and Liquids. Wiley, New York.

HÖCKER, K.H. and KLUGE, W., 1959: Proc. IV. Int. Conf. Ionization Phenomena in Gases, 904, Uppsala.

JACKSON, E.A., 1960: Phys. of Fluids, Vol. 3 Nr. 5

KAEPPELER, H.J., 1958: Mitt. Forsch. Inst. Phys. Strahlantriebe Nr. 15 Stuttgart

KLUGE, W. and K.H. HÖCKER, 1960: Ohmic Heating of Fully Ionized Plasmas, ARL-60-172 (Technical Note)

KLUGE, W. and W. THIELO, 1961: Proc. V. Int. Conf. on Ionization Phenomena in Gases, München

KNORR, G., 1958: Z. Naturforsch. 13a, 941

MAIER, H.H., H.G. HARTNER and E. PFENDER, 1960: A.E.Ü. Heft 14, 515-519

MAILÄNDER, M., 1961: Diplomarbeit, Inst. für Hochtemperaturforschung, T.H. Stuttgart.

MAISENHÄLDER, F., PURPS, H.D. and PFENDER, E., 1961: Arch. d. Elektr. Übertragungen 15, 253.

PFENDER, E. and W. BEZ, 1961: Proc. V. Int. Conf. on Ionization Phenomena in Gases, Vol. I, München.

PFENDER, E., 1962: A high temperature-high density hydrogen plasma, Res. Rev. OAR Nr. 8, 4

References, continued:

SCHNEIDER, R. and M. MAILÄNDER, 1961a: Z.f. angew. Phys. 12, 521

SCHNEIDER, R., F. MAISENHÄLDER and M. KLING, 1961b: Z.f.angew. Phys. 13, 211.

SCHNEIDER, R., 1961c: Dissertation T.H. Stuttgart, s.a. Proc. V. Int. Conf. on Ionization Phenomena in Gases.

SCHRADE, H., W. BEZ, K.H. HÖCKER and H.J. KAEPPELER, 1960: Z. Naturforsch. 15a, 155

SCHRADE, H., 1963: Dissertation, T.H. Stuttgart, Technical Note to Contract AF 61 (052)-590 "Ohmic Heating of Hydrogen Plasmas".

SCHRADE, H., 1961: Proc. V. Int. Conf. on Ionization Phenomena in Gases, Vol. 2, München.

THIELO, W., 1963: Dissertation T.H. Stuttgart, Technical Note to Contract AF 61 (052)-590 "Investigation of a high density nitrogen plasma by means of magnetic probes".

TIDMAN, D.A., 1961: Phys. of Fluids, Vol. 4 Nr. 11

UNSÖLD,A., 1955: Phys. der Sternatmosphären, Springer, Berlin

WILHELM, H.E., 1962: Nuclear Fusion, Vol. 1 Nr. 1

ZIMMERMANN W. and H.J. KAEPPELER, 1962: Equilibrium Composition and Thermodynamic Functions of Nitrogen Plasmas, Contract AF 61 (052)-199.

Aeronautical Research Laboratories, Wright-Patterson AFB,O. TRANSIENT DISCHARGES IN WHIRL STABILIZED ARCS by K.H. Hocker, et al, Technishen Hochschule, Stuttgart, Germany. June 1963. 79 p. incl.illus. (Project 7073;Task7073-01) (Contract AF 61 (052)-590) (ARL 63-105)
Unclassified Report

Experiments were conducted to study the problem of heating and stability of pulsed discharges. In order to have reproducible conditions and defined geometry a pre-discharge representing a highly ionized plasma

(over)

UNCLASSIFIED

was used and described. Then, the basic equations for the heating process which were developed in our institute and the main features of a model which allows to apply them to a cylindrical discharge are summarized.

UNCLASSIFIED

Aeronautical Research Laboratories, Wright-Patterson AFB,O. TRANSIENT DISCHARGES IN WHIRL STABILIZED ARCS by K.H. Hocker, et al, Technishen Hochschule, Stuttgart, Germany. June 1963. 79 p. incl.illus. (Project 7073;Task7073-01) (Contract AF 61 (052)-590) (ARL 63-105)
Unclassified Report

Experiments were conducted to study the problem of heating and stability of pulsed discharges. In order to have reproducible conditions and defined geometry a pre-discharge representing a highly ionized plasma

(over)

UNCLASSIFIED

was used and described. Then, the basic equations for the heating process which were developed in our institute and the main features of a model which allows to apply them to a cylindrical discharge are summarized.

UNCLASSIFIED